Published in "Biochimica et Biophysica Acta (BBA) - Molecular Cell Research 1853(3): 632–645, 2015" which should be cited to refer to this work.

Characterization and modeling of Ca^{2+} oscillations in mouse primary mesothelial cells

László Pecze, Beat Schwaller *

Anatomy, Department of Medicine, University of Fribourg, Route Albert-Gockel 1, CH-1700 Fribourg, Switzerland

Brief changes in the cytosolic and intra-organellar Ca^{2+} concentration serve as specific signals for various physiological processes. In mesothelial cells lining the surface of internal organs and the walls of body cavities, a re-entry in the cell cycle (G_0–G_1 transition) evoked by serum re-administration induces long-lasting Ca^{2+} oscillations with a slowly decreasing frequency. Individual mesothelial cells show a wide range of different oscillatory patterns within a single, supposedly homogenous cell population. Changes in the cytoplasmic Ca^{2+} concentration (c_{cyt}) show baseline oscillatory patterns i.e., discrete Ca^{2+} transients starting from a constant basal c_{cyt} level. The ER Ca^{2+} concentration (c_{ER}) displays a sawtooth wave at a semi-depleted ER state; the minimum level is reached just briefly after the maximal value for c_{cyt}. These oscillations depend on plasmalemmal Ca^{2+} influx and on the inositol trisphosphate concentration [$InsP_3$]; the Ca^{2+} influx is a crucial determinant of the oscillation frequency. Partial blocking of SERCA pumps modifies the oscillation frequency in both directions, i.e. increasing it in some cells and lowering it in others. Current mathematical models for Ca^{2+} oscillations mostly fail to reproduce two experimentally observed phenomena: the broad range of interspike intervals and constant basal c_{cyt} levels between two Ca^{2+} spikes. Here we developed a new model based on – and fitted to – Ca^{2+} recordings of c_{cyt} and c_{ER} recorded in primary mouse mesothelial cells. The model allowed for explaining many features of experimentally observed Ca^{2+} oscillations. We consider this model to be suitable to simulate various types of $InsP_3$ receptor-based baseline Ca^{2+} oscillations.

1 . Introduction

Mesoderm-derived mesothelial cells cover the body's serous cavities (pleural, pericardial and peritoneal) and internal organs. They have a flattened, simple squamous epithelial morphology possessing microvilli and cilia on their luminal surface and express both mesenchymal and epithelial cell intermediate filaments. Under normal physiological conditions, the mesothelium is a slowly renewing tissue with 0.16–0.5% of cells undergoing mitosis, i.e. most cells are in a quiescent (G_0) state [1]. Mesothelial cells secrete glycosaminoglycans, proteoglycans and phospholipids forming the lubricant that reduces the friction between organs and serosal surfaces. The cells are also involved in transport across serosal cavities, antigen presentation, inflammation and tissue repair, coagulation and fibrinolysis [1,2].

Only few studies have investigated Ca^{2+} signals in primary mesothelial cells (prMC). Such transient Ca^{2+} signals were observed after acute acidification [3], histamine administration [4], serum re-administration [4], ryanodine treatment [5], platelet-derived growth factor administration [6] and K^+-induced membrane depolarization [5]. However, Ca^{2+} signals in the form of oscillations have not been reported previously.

* Corresponding author. Tel.: +41 26 300 85 08; fax: +41 26 300 97 33.
E-mail address: Beat.Schwaller@unifr.ch (B. Schwaller).

When cells transit from a quiescent state (G_0) and re-enter the cell cycle during tissue remodeling and repair [7], this transition is generally associated with Ca^{2+} signals, most often in the form of oscillations [8,9]. Depending on the shape and length of these oscillations, different types can be distinguished including sinusoidal and baseline spiking oscillations. The baseline spiking oscillations represent discrete Ca^{2+} transients starting from a constant basal c_{cyt} level. Sinusoidal oscillation is a term for a continuous fluctuation in the cytoplasmic Ca^{2+} concentration (c_{cyt}) starting from a c_{cyt} value that is higher than the resting c_{cyt}. Most probably, sinusoidal oscillations are the result of high-frequency overlapping baseline spiking oscillations [10]. The resting c_{cyt} level represents c_{cyt} before the administration of an inducer of oscillations. The basal c_{cyt} denotes a constant c_{cyt} level observable during the interspike period; the resting and the basal c_{cyt} may be different, most often basal c_{cyt} is lower than resting c_{cyt} in mesothelial cells. A G_0–G_1 cell cycle transition with the associated Ca^{2+} transients can be mimicked in vitro by serum deprivation followed by serum re-administration. Serum contains a plethora of known and as-yet-unidentified growth factors and mitogenic compounds [11]. These factors promote the cell to pass from G_0 through G_1 to the DNA synthesis (S) phase. The stimulation of DNA synthesis usually requires the simultaneous action of at least two growth factors or mitogens. In Swiss 3T3 fibroblasts, the epidermal growth factor (EGF) and insulin are the best-characterized combination

[12]. Studies revealed that the separate administration of either platelet-derived growth factor, vasopressin, prostaglandin, bombesin or EGF evokes Ca^{2+} transients and also induces inositol trisphosphate ($InsP_3$) production [13,14]. In Swiss 3T3 cells, serum-induced Ca^{2+} increases are essential, but not sufficient to induce NF-κB activation and subsequent DNA synthesis [15]. Hormone receptors, for example EGF receptor, activate phospholipase C [16] that causes the hydrolysis of phosphatidylinositol bisphosphate to $InsP_3$ and diacylglycerol (DAG) [17]. The molecular identity of the ion channels mediating hormone-induced Ca^{2+} entry in mesothelial cells is still unknown. Most probably transient receptor potential canonical (TRPC) channels are involved, because these channels are activated by DAG [18]. On the other hand, a drop in the Ca^{2+} concentration in the lumen of the ER (c_{ER}) after hormonal stimulation activates store-operated Ca^{2+} channels (SOC). STIM molecules function as Ca^{2+} sensors in the ER membrane, interact with and activate plasmalemmal Orai Ca^{2+} channels [19]. Both $InsP_3$ production and Ca^{2+} influx play an essential role in hormone-induced Ca^{2+} oscillations examined in many non-excitable cell types, for instance, in microvascular endothelial cells [20], in astrocytes [21] and in pre-adipocytes [22].

However, despite the effort made to understand the mechanism of Ca^{2+} oscillations, there is still a lot of debate and controversy. First of all, there is no mathematical model, which can recapitulate the various patterns of Ca^{2+} oscillations observable even in a homogenous population of cells growing in cell culture. Here, we investigated Ca^{2+} oscillations in mouse prMC elicited by serum re-administration using genetically encoded Ca^{2+} indicators. Based on the time-lapse recordings of c_{cyt} and c_{ER} in these cells, we built up a new model for Ca^{2+} oscillations. This model accomplished to answer many questions on typical features of these Ca^{2+} oscillations recorded in prMC such as: Why does c_{cyt} show a baseline oscillatory pattern, while changes in c_{ER} are characterized by a sawtooth wave starting from a semi-depleted ER state? Why do the oscillations stop/subside when decreasing the extracellular Ca^{2+} concentration? How do these oscillations change when partially blocking the function of sarcoendoplasmic reticulum Ca^{2+}-ATPases (SERCA)?

2 . Material and methods

2.1. Reagents

Thapsigargin (THAPS), carbenoxolone, N-methyl-D-glucamine and EGTA were purchased from Sigma Aldrich (St. Louis, MO, USA). Ionomycin (IONO), SKF 96365 hydrochloride, ryanodine, ML-9, U73122, BAPTA-AM were obtained from Tocris Bioscience (Bristol, UK) and Ru360 from Calbiochem (San Diego, CA).

2.2. Primary mesothelial cell isolation

Mesothelial cells were isolated from 4–6 months old C57Bl/6J mice (C57) according to an established protocol [23]. Briefly, mice were sacrificed by cervical dislocation. The abdominal wall was exposed by incision into the fur and removal of it. The peritoneal cavities were washed with injecting approximately 50 ml of PBS (Sigma, St. Louis) via a 25G needle using a peristaltic pump and a second 21G needle to allow exit of the PBS solution until it was clear, i.e. devoid of mobile and poorly attached cells. Residual PBS was aspired with a syringe and the peritoneal cavity was filled with 5 ml of 0.25% Trypsin/EDTA solution (Sigma Aldrich). The body temperature of mouse corpses was maintained at around 37 °C via an infrared heating lamp for 10 min. The suspension containing the detached cells was collected with a syringe, cells were centrifuged for 10 min at 300 × *g*. Cells mostly comprising primary mesothelial cells were grown in DMEM/F12 GlutaMax medium supplemented with 15% FCS, 0.4 mg/ml hydrocortisone, 10 ng/ml epidermal growth factor, 1% ITS (insulin, transferrin, selenium), 1 mM sodium pyruvate, 0.1 mM beta-mercaptoethanol, 1% non-essential amino acids, 1% Penicillin–Streptomycin and 2% Mycokill (PAA Laboratories, Pasching, Austria) [24]. Cultures showing typical cobblestone morphology were used for measurements.

2.3. Plasmids and lentiviral infection

For the generation of primary mesothelial cell lines stably expressing the Ca^{2+} indicator proteins, GCaMP3 (Addgene plasmid 22692 [25]), GEM-GECO1 (Addgene Plasmid 32442 [26]) and D1ER (Addgene 36325 [27]), the lentiviral expression vector pLVTHM (Addgene plasmid 12247 [28]) was used. The GFP cassette in pLVTHM was replaced with cDNAs coding for the respective Ca^{2+} indicator proteins. Briefly, pGCaMP3 was grown in SCS110 dam$^-$ bacteria, digested with *AfeI* and *XbaI* and the fragment was inserted into the compatible *PmeI* and *SpeI* sites of the backbone of pLVTHM to produce the final pLV-GCaMP3. The pCMV-GEM-GECO1 was digested with *BamHI*, filled with Klenow enzyme, and then digested with *XbaI*. The cDNA insert was ligated into pLVTHM using the compatible *PmeI* and *SpeI* sites. The plasmid pcDNA-D1ER was grown in SCS110 dam$^-$ bacteria, digested with *HindIII*, filled with Klenow enzyme, digested with *XbaI* and ligated into the compatible *PmeI* and *SpeI* sites of pLVTHM. All lentiviral plasmids were verified by restriction enzyme digestion. Lentivirus was produced by the calcium phosphate transfection method using HEK293T cells and three plasmids: one of the expression plasmids (pLV-GCaMP3, pLV-GEMGECO1, pLV-D1ER), the envelope plasmid (pMD2G-VSVG Addgene plasmid 12259) and the packaging plasmid (pCMV-dR8.91, a kind gift from Prof. D. Trono (EPFL, Lausanne)). Viral supernatants were collected after 48 h and 72 h, filtered, aliquoted and frozen at −80 °C [29].

2.4. Calcium imaging

Mesothelial cells were grown on collagen-coated glass bottom 35 mm dishes (MatTek Corp., Ashland, MA). The buffer solution (DPBS) used for Ca^{2+} imaging experiments contained (in mM): NaCl 138, Na_2HPO_4 8, $CaCl_2$ 2, $MgCl_2$ 0.5, KCl 2.7, KH_2PO_4 1.6, and pH 7.4. In the low Ca^{2+} solution, $CaCl_2$ was replaced with an equimolar concentration of NaCl. In the low Na^+ solution, NaCl and Na_2HPO_4 were replaced with an equimolar concentration of N-methyl-D-glucamine. The drugs (THAPS, FCS, IONO, Pyr3, SKF 96365, ryanodine, ML-9) were added to the above-mentioned solutions and remained in the solution until the end of the experiments. In some experiments, cells were pre-treated either with 250 μM carbenoxolone or with 10 μM Ru360 for 30 min at 37 °C.

We used an inverted confocal microscope DMI6000 integrated to a Leica TCS-SP5 workstation to examine fluorescence signals indirectly reporting c_{cyt} or c_{ER}. The following excitation wavelengths were used to illuminate the fluorophores: 488 nm for GCaMP3, 404 nm for GEM-GECO1 and 455 nm for D1ER. Fluorescence emissions were recorded with a 20× objective and bandpass filters of 505–550 nm for GCaMP3, 425–490 nm simultaneously with 520–575 nm for GEM-GECO1 or 460–508 nm simultaneously with 515–565 nm for D1ER. Fluorescence images for c_{cyt} or c_{ER} measurements were collected every 3 s. Circular-shaped regions of interest (ROI) were placed inside the cytoplasmic area of cells. The fluorescence values were calculated after background subtraction (fluorescence intensity of regions without cells). In the case of GCaMP3, fluorescence intensity values were normalized in each experiment to the averaged basal value preceding the treatment period.

The absolute c_{cyt} was calculated using the fluorescent Ca^{2+} indicator GEM-GECO1. GEM-GECO1 ratios were converted to Ca^{2+} concentrations using the equation:

$$c_{cyt} = \left(K_d{}^{H} * (R - R_{min})/(R_{max} - R)\right)^{1/H} \quad (1)$$

where K_d is the apparent dissociation constant ($K_d = 340$ nM) and H is the Hill coefficient ($H = 2.94$) [26]; R_{max} is the maximal fluorescence

ratio obtained after ionomycin (30 μM) treatment ($[Ca^{2+}]_o \approx 1$ mM), R_{min} is the experimental minimal fluorescence ratio obtained during ionomycin (10 μM) treatment in an extracellular solution containing 50 mM EGTA.

The absolute c_{ER} was calculated using the FRET-based Ca^{2+} indicator D1ER. FRET ratios were converted to Ca^{2+} concentrations using the equation:

$$c_{ER} = K_d * ((F - F_{min})/(F_{max} - F))^{1/H} \quad (2)$$

where K_d is the low affinity dissociation constant ($K_d = 200$ μM), H is the Hill coefficient ($H = 1.67$), F is the YFP/CFP ratio, F_{min} is the minimal ratio after the treatment of ionomycin (1 μM) and EGTA (50 mM), The D1ER Ca^{2+} indicator has biphasic Ca^{2+}-binding kinetics with K_d values of 0.81 and 69 μM, and Hill coefficients of 1.18 and 1.67, respectively based on in vitro calibration data [27]. Based on the assumption that c_{ER} is not expected to fall below 1 μM, we ignored the high affinity K_d of D1ER, in line with previous studies, e.g. [30]. Furthermore, we chose to use the in vivo measured value for the low affinity K_d [30], which is three-fold higher than the one calculated in vitro [27]. The noise was reduced using a rolling average method with a window size of 3. The LAS-AF (Leica) and Prism5 (*GraphPad* Software, Inc., San Diego, CA) software were used for data analysis.

2.5. Frequency and amplitude scan

Computerized peak recognition for frequency and amplitude scans was achieved by using the Microsoft Excel 2010 environment. Normalized recordings from 100 oscillating GCaMP3-expressing prMC were evaluated. A peak was recognized and the number 1 was assigned, if the respective relative fluorescence value was higher than that of the neighboring values. In order to avoid the peaks produced by noise, this value needed to be higher than the average of the surrounding 10 values. In all other cases, the number 0 was assigned. This method allowed us to separate the real Ca^{2+} spikes from small peaks derived from noise. Summing up the assigned numbers during a time interval (30 s) allowed for measuring the number of spikes and calculating the frequency scan. To perform the amplitude scans, the relative fluorescence values were assigned to each spike in a certain time interval (30 s). Then, the average peak amplitude was calculated.

2.6. Building up the model

To build up the mathematical model, we considered only three compartments: the extracellular space, the cytoplasm and the ER lumen. Endoplasmic reticulum–plasma membrane junctions ensure that the functional unit components (Ca^{2+} channels and pumps) are concentrated spatially in a very small space [31]. We assume that changes in c_{cyt} or c_{ER} of the entire cell are similar to that of individual units, i.e. spatially homogenous. In our view, this simplification is acceptable, since the oscillations are slow and the cell size is small. In this case the spatial diffusion of Ca^{2+} will equilibrate the spatial differences and thus synchronizes the functions of individual functional units [32]. In a cell with a 10-μm diameter, the diffusion is estimated to equilibrate spatial heterogeneity in c_{cyt} in less than 0.1 s [33]. However, because the Ca^{2+} wave not only depends on Ca^{2+} diffusion, but also on the action of Ca^{2+} pumps and channels the Ca^{2+} wave is approximately 10 times slower [34]. At higher frequencies the synchronization between the individual oscillatory units is lost producing overlapping and finally irregular Ca^{2+} waves in the cell [35].

Ca^{2+} transport across the plasma membrane was defined as IN and EFF, and the transports across the ER membrane were termed SERCA and EREFF, respectively. IN includes Ca^{2+} channels in the plasma membrane: e.g. voltage-gated Ca^{2+} channels (VGCC), transient receptor potential channels (TRP channels), SOC (store-operated channels), P2X purinoreceptors, hyperpolarization-activated cyclic nucleotide-gated channels (HCN channels), etc. The EFF represents the pumps involved in Ca^{2+} extrusion: PMCA (plasma membrane Ca^{2+} ATPases) and NCXs (Na^+–Ca^{2+} exchangers). The SERCA pumps transport Ca^{2+} from the cytoplasm to the ER, while the EREFF represents the ER channels involved in emptying the ER: RyR (ryanodine receptors) and $InsP_3Rs$ (inositol trisphosphate receptors) (Fig. 1).

We denote by c_{cyt} the Ca^{2+} concentration (in nM) in the cytosol and by c_{ER} the one in the lumen of the ER. The equations for the model are:

$$\frac{dc_{cyt}}{dt} = J_{IN} - J_{EFF} - J_{SERCA} + J_{EREFF} + J_{ERLEAK} \quad (3)$$

$$\frac{dc_{ER}}{dt} = \gamma(J_{SERCA} - J_{EREFF} - J_{ERLEAK}) \quad (4)$$

where J_{IN} is the amount of Ca^{2+} entering the cell, J_{EFF} the Ca^{2+} quantity pumped out of the cell, J_{SERCA} denotes the amount of Ca^{2+} pumped from the cytosol to ER, J_{EREFF} the flux of Ca^{2+} passing from the ER to the cytosol and finally J_{ERLEAK} represents a small flux of Ca^{2+} diffusing from the ER to the cytosol, (all values in nM/s).

The constant γ is the ratio between the changes in c_{cyt} and c_{ER} caused by the same quantity of Ca^{2+} ions transported through the ER membrane. This value is derived from the difference in the effective volume of the ER lumen and the cytoplasm and from the different fraction of free and protein-bound Ca^{2+} in these compartments:

$$\gamma = V_{cyt} * f_{ER}/V_{ER} * f_{cyt} \quad (5)$$

where, V_{cyt} is the effective volume of the cytoplasm, V_{ER} is the effective volume of the ER, f_{ER} and f_{cyt} are the fractions of free Ca^{2+} in cytoplasm and ER [36]. The value of the γ parameter was estimated experimentally. The Ca^{2+} peak in the cytoplasm evoked by ionomycin is mainly due to the depletion of ER stores. Ionomycin depletes approximately 80–90% of the ER Ca^{2+}. This causes en elevation in c_{cyt}. Thus, the γ parameter can be estimated according to the following equation:

$$\gamma = (c_{ERb} - c_{ERa})/\left(c_{cytm} - c_{cytb}\right) \quad (6)$$

where c_{ERb} is the c_{ER} before ionomycin treatment, c_{ERa} is the c_{ER} after ionomycin treatment, c_{cytm} is the maximal c_{cyt} after ionomycin treatment, c_{cytb} is the c_{cyt} before ionomycin treatment (all values in nM). However, the measured c_{cytm} is influenced by the Ca^{2+} extrusion system (EFF) resulting in a slight overestimation of the γ value.

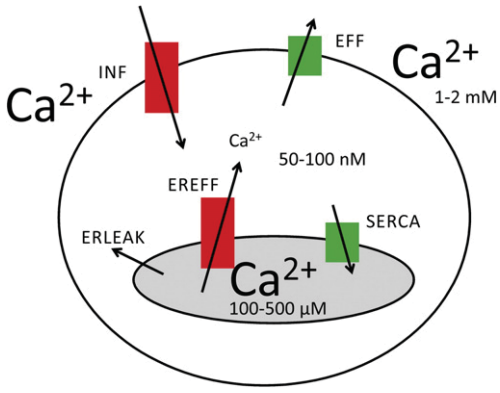

Fig. 1. Schematic model of cellular compartments implicated in Ca^{2+} oscillations in mouse primary mesothelial cells. The plasma membrane contains components responsible for Ca^{2+} influx (IN) and efflux (EFF). The relevant intracellular Ca^{2+} release (EREFF) and uptake (SERCA) systems are localized in the ER membranes. Values of Ca^{2+} concentrations in the extracellular space, the cytoplasm and in the ER lumen are given. A small constant leak (ERLEAK) occurs independently of Ca^{2+} channels.

The quantity of Ca^{2+} pumped out the cell through the plasma membrane increases as a function of the Ca^{2+} concentration in the cytosol. Although the individual components (NCXs and PMCAs) of extrusion systems are usually modeled by Hill equations [37], the overall flux can be simulated by a simple linear equation [38] based on the experimental results of Herrington et al. [39]. The advantage of the linear flux simulation is that it does not have a saturation concentration. The different K_d values of individual components (PMCAs and NCXs) ensure that the extrusion flux will never reach its saturation point in the range of biologically relevant values of c_{cyt}.

$$J_{EFF} = \begin{cases} 0, r_{e_1} c_{cyt} - r_{e_2} \le 0 \\ r_{e_1} c_{cyt} - r_{e_2}, r_{e_1} c_{cyt} - r_{e_2} > 0 \end{cases} \quad (7)$$

where r_{e_1} and r_{e_2} are two positive constants.

SERCAs pump the Ca^{2+} ions from the cytosol to ER. The quantity of the transported Ca^{2+} ions depends on c_{cyt} levels. We assume a linear relationship, because the ER influx is also composed of different SERCA pumps with different K_d values [40]. Nevertheless, our model can also work when EFF or/and SERCA fluxes were simulated with the conventional Hill equations. The rather limited number of experimental data [41] shows that SERCA function depends not only on c_{cyt}, but also on c_{ER}. This is likely the case for a resting state, when the c_{ER} is high, however during the Ca^{2+} oscillations the ER is in a semi-depleted state. Because in this semi-depleted state c_{ER} has essentially no or only a minimal influence on SERCA activity [41], the SERCA dependence on c_{ER} was not implemented into the model.

$$J_{SERCA} = \begin{cases} 0, r_{s_1} c_{cyt} - r_{s_2} \le 0 \\ r_{s_1} c_{cyt} - r_{s_2}, r_{s_1} c_{cyt} - r_{s_2} > 0 \end{cases} \quad (8)$$

where r_{s_1} and r_{s_2} are two positive constants.

Ca^{2+} ions are released from the ER to the cytosol through $InsP_3R$ and RyR. Because we found experimentally that RyR does not play a role in serum-induced oscillations in mesothelial cells similarly to other non-excitable cells [42], we focused on $InsP_3R$. In our model, $InsP_3Rs$ are influenced both by c_{cyt} and by c_{ER}, however without an allosteric regulation between the two. $InsP_3Rs$ have Ca^{2+} binding sites not only on the cytoplasmic side, but also on the luminal side [43]. Experimental data show that an increase in $[InsP_3]$ causes a significant Ca^{2+} release from the ER in the absence of cytosolic Ca^{2+} ($c_{cyt} = 0$) [44]. Moreover, the effects of luminal Ca^{2+} do not affect the cytosolic binding sites [45,46]. Therefore we modeled $InsP_3R$ function as the sum of two individual contributions:

$$J_{EREFF} = \begin{cases} 0, J_{cytdep} + J_{ERdep} \le 0 \\ J_{cytdep} + J_{ERdep}, J_{cytdep} + J_{ERdep} > 0 \end{cases} \quad (9)$$

where

$$J_{cytdep} = r_{i,max} exp\left(- \frac{\left(\log\left(c_{cyt}\right) - \mu \right)^2}{\sigma^2} \right) \quad (10,\ 11)$$

$$J_{ERdep} = r_{i1} log(c_{ER}) - r_{i2}$$

with positive constants σ and r_{i_1}.

We introduced the dependence of $InsP_3R$ on the $InsP_3$ concentration ($[InsP_3]$), which has an influence both on J_{cytdep} and on J_{ERdep}. According to the experimental data from several studies [47–49], elevating $[InsP_3]$ mainly changes the mean and the maximum (μ, $r_{i,max}$) of the bell-shaped curve of c_{cyt} dependence. Nevertheless, based on the experimental data presented in [50,51], elevating $[InsP_3]$ also has an effect on the loading of the ER. Increased $[InsP_3]$ reduces the amount of the stored Ca^{2+} ions. We simulated this effect by changing the r_{i2} parameter:

$$\mu = \mu_{min} + (\mu_{max} - \mu_{min}) \frac{K_b}{K_b + [InsP_3]} \quad (12)$$

$$r_{i,max} = r_{im,min} + \left(r_{im,max} - r_{im,min} \right) \frac{K_b}{K_b + [InsP_3]} \quad (13)$$

$$r_{i2} = r_{i2,min} + \left(r_{i2,max} - r_{i2,min} \right) \frac{K_b}{K_b + [InsP_3]} \quad (14)$$

where K_b is the half-saturation constant of $InsP_3R$ for $InsP_3$ and $[InsP\ 3]$ represents the inositol-trisphosphate concentration in μM. μ_{max}, μ_{min}, $r_{im,min}$, $r_{im,max}$, $r_{i2,min}$, and $r_{i2,max}$ are positive constants. The parameter J_{ERLEAK} accounts for a Ca^{2+} flux from the ER to the cytoplasm independently of known Ca^{2+} channels and this parameter is assumed to represent a small constant value [52].

$$J_{ERLEAK} = \beta \quad (15)$$

The values of each parameter are listed in Table 1. The initial values of parameters are derived either from our experiments in primary mesothelial cells or from fitting to experimental data previously reported in the above-mentioned articles. The presented values are the result of the sequential fitting of the initial values to our in situ recordings.

The Ca^{2+} influx across the plasma membrane is composed of a passive leakage and the agonist-activated fluxes: the capacitive (SOC-dependent) and the non-capacitive (arachidonate or DAG regulated) Ca^{2+} influx [53]. We simulated the changes in J_{IN} starting from the beginning of the administration of serum (t_1) using the following equations:

$$J_{IN} = 0.1 \text{ nM/s, if } t < t_1 \text{ (only passive leakage)} \quad (18)$$

$$J_{IN} = r_{IN,MAX} \frac{(t - t_1)}{K_{IN,1} + (t - t_1)}, \text{ if } t_1 \le t \le t_2 \quad (19)$$

$$J_{IN} = \left(r_{IN,MAX} - r_{IN,p} \right) * \exp\left(-K_{IN,2}(t - t_2) \right) + r_{IN,p}, \text{ if, } if\ t > t_2. \quad (20)$$

Table 1
Parameters used for the modeling.

Equation to determine	Parameter name	Value
J_{EFF} (Eq. (7))[a]	γ	450
	r_{e_1}	0.17/s
	r_{e_2}	18.8 nM/s
J_{SERCA} (Eq. (8))[a]	r_{s_1}	0.27/s
	r_{s_2}	22 nM/s
J_{EREFF} (Eq. (9))	σ	0.14142 nM
	r_{i_1}	1300/s
μ (Eq. (12))	μ_{min}	2.4 nM
	μ_{max}	2.18 nM
	K_b	2 μM
$r_{i,max}$ (Eq. (13))	$r_{im,\ min}$	821.3 nM/s
	$r_{im,max}$	24.3 nM/s
	K_b	2 μM
r_{i_2} (Eq. (14))	$r_{i2,min}$	6352 nM/s
	$r_{i2,max}$	7042 nM/s
	K_b	2 μM
J_{ERLEAK} (Eq. (15))	β	2.5 nM/s
	c_{ER}(initial)	260 μM
	c_{cyt}(initial)	110 nM

[a] Alternatively, J_{EFF} and J_{SERCA} can be simulated conventionally with a Hill equation with the following parameters: V_{max} 260 nM/s and 170 nM/s, K_d 460 nM and 480 nM, and Hill coefficients of 3.5 and 2.4, respectively.

We simulated the changes in $[InsP_3]$ from the beginning of the administration of serum ($t1$) with the following equations. The resting $[InsP_3]$ was set to 15 nM [54]:

$$[InsP_3] = 0.015,\ if\ t<t_1 \tag{21}$$

$$[InsP_3] = i_{IP3,MAX}\frac{(t-t_1)}{K_{IP3}+(t-t_1)},\ if\ t\geq t_1 \tag{22}$$

The values for the above parameters are reported in the figure legends for each simulation.

All computations of the model were implemented in the Microsoft Excel 2010 environment. The model system was discretized with a temporal resolution of 0.1 s (Supplementary Excel document). There were no significant differences in the solution of the differential equations, if we increased the temporal resolution (not shown). For the visualization, Prism5 (GraphPad Software, Inc., San Diego, CA) software was used.

3 . Results

3.1. Characterization of serum-induced Ca^{2+} oscillation in mesothelial cells

Primary mouse mesothelial cells (prMC) maintained in the absence of serum in the medium for 24 h responded to the addition of 10% FCS to the cell culture medium with a sudden rise of c_{cyt} lasting for approximately 40 s, followed by Ca^{2+} oscillations (Fig. 2A and Supplementary movie) in approximately 70% of cells. The Ca^{2+} responses in individual mesothelial cells showed a wide range of different oscillatory patterns that were elicited in a presumably homogenous population of mesothelial cells. Most cells displayed long-period (>10 min) baseline spiking oscillations, while some cells initially showed few short-period sinusoidal, i.e. overlapping baseline oscillations before changing to baseline spiking oscillations. In prMC cultured for longer periods (>10 passages) the duration of the sinusoidal oscillations was increased, however the fraction of cells showing baseline spiking oscillations was strongly reduced. The frequency and the amplitude scans from oscillating prMC revealed that the amplitude didn't change in the time period from 2 to 13 min after serum re-administration, while the oscillation frequency decreased during this time period (Fig. 2B). During oscillations the Ca^{2+} spike amplitudes reached c_{cyt} values ranging from 140 to 250 nM as measured with the GEM-GECO1 indicator; resting c_{cyt} was between 80–120 nM and basal c_{cyt} during the baseline oscillations was usually slightly lower (Fig. 3), calculated to be in the order of 80–100 nM. Using a FRET-based Ca^{2+} indicator D1ER, the resting c_{ER} was found to be in the order of 150–250 μM and serum re-administration caused a reduction in c_{ER} to 100–150 μM. The pattern of c_{ER} changes is best described as a sawtooth wave (Fig. 2C).

Ca^{2+} waves propagating from one cell to the next possibly via gap junctions were sometimes observed; the presence of connexin 43 in mesothelial cells allowing for the transfer of Ca^{2+} ions or other low-molecular weight molecules (e.g. $InsP_3$) between connected cells has been reported before [55]. Since Ca^{2+} oscillations persisted in cell cultures pre-treated with carbenoxolone, a gap junction blocker [56] (data not shown), we considered Ca^{2+} and/or $InsP_3$ fluxes through gap junctions not essential for oscillations and we didn't implement these mechanisms in our model. Similarly we did not consider the function of mitochondria as putative Ca^{2+} stores or sources in our model, since pretreatment of the cells with Ru360, a cell-permeable mitochondrial Ca^{2+} uptake blocker [57], did not inhibit Ca^{2+} oscillations (data not shown).

With the aim to investigating the role of RyRs in mesothelial cell Ca^{2+} oscillations, cells were exposed to a high concentration of ryanodine (50 μM); ryanodine fully closes RyRs at micromolar concentrations [58]. In most cells ryanodine did not affect serum-induced Ca^{2+} oscillations (Fig. 2D), but in some cases transiently and slightly reduced the frequency of oscillations together with a short-lasting lowering of basal c_{cyt}. Thus, RyRs appeared to be minimally implicated in Ca^{2+} oscillations in prMC. Preventing $InsP_3$ production by the phospholipase C inhibitor U-73122, the serum-induced oscillations in prMC were blocked indicating that these oscillation are essentially based on elevated $[InsP_3]$ (Fig. 2E). Lower serum concentration resulted in a decreased oscillation frequency. The duration of oscillations was shorter and c_{ER} recovered faster from its semi-depleted ER state (Fig. 2F).

Based on previous findings that human mesothelioma, mesothelioma cells in vitro and reactive mesothelial cells express calretinin [59,60], an EF-hand with complex binding kinetics [61], we hypothesized that also murine mesothelial cells might express this protein and that its presence might affect the Ca^{2+} oscillations. However, calretinin protein expression levels in mouse primary mesothelial cells were found to be below the detection limit of our Western blot analysis [62], i.e. lower than approximately 100 nM, thus unlikely to affect the oscillations. In support the oscillation patterns (frequency, amplitude, duration) in primary mesothelial cells derived either from calretinin knockout (CR−/−) or from wildtype mice were indistinguishable (data not shown). Nevertheless, the effect of a synthetic fast buffer, BAPTA (K_d = 0.2 μM; k_{on} = 500 $\mu M^{-1}\ s^{-1}$), was tested; BAPTA significantly reduced the amplitude of Ca^{2+} oscillations, but broadened (increased half-width) the Ca^{2+} transients (Fig. 2G). A similar effect had been modeled for repetitive (20 Hz) Ca^{2+} transients in dendrites of neurons with or without BAPTA (see Fig. 3 in [61]).

The Ca^{2+} efflux is mediated by PMCAs and NCXs. The NCXs have low Ca^{2+} affinities, but high capacity for Ca^{2+} transport, whereas the PMCAs have a high Ca^{2+} affinity, but a low transport capacity [63]. Despite the low Ca^{2+} affinity of NCXs, they play an important role in the Ca^{2+} efflux in primary mesothelial cells. NCXs use the energy that is stored in the electrochemical gradient of Na^+ by allowing Na^+ to flow down its gradient across the plasma membrane in exchange for the counter transport of Ca^{2+} ions. Thus, the removal of Na^+ ions from the extracellular space was assumed to impair the function of NCXs and to reduce the Ca^{2+} efflux. Consequently, replacing the extracellular Na^+ ions with N-methyl-D-glucamine strongly inhibited Ca^{2+} oscillations (Fig. 2H).

3.2. Modeling the effect of serum re-administration on cytoplasmic and luminal $[Ca^{2+}]$ in primary mesothelial cells

In mesothelial cells, serum re-administration induced both, Ca^{2+} influx through the plasma membrane and Ca^{2+} release from the ER due to $InsP_3$ production. Therefore, both independent variables (J_{IN} and $[InsP_3]$) changed after serum re-administration. We selected two recordings showing oscillations, one with a small amplitude and one with a big amplitude. Fitting our model to these recordings revealed that these oscillations are essentially based on different $[InsP_3]$, i.e. $i_{IP3,MAX}$ is either 0.24 μM (Fig. 3A) or 1.8 μM (Fig. 3B and Supplementary Excel document). Nevertheless, we can't exclude that differences in the Ca^{2+} efflux activities between these two cells might also contribute to the differences in amplitudes.

The model also predicted that serum-induced stimulation of prMC causes a partial depletion of c_{ER} and a sawtooth wave starting at c_{ER} lower than basal c_{ER} (Fig. 3A, B; lower traces). This is exactly in line with the experimental findings (Fig. 2C).

3.3. Pharmacological identification of Ca^{2+} influx components and modeling the effect of the magnitude of Ca^{2+} influx (J_{IN}) on the oscillation frequency

Ionomycin is a Ca^{2+} ionophore forming pores in cell membranes. At low concentrations (≤500 nM) ionomycin evokes a transient Ca^{2+} signal that mostly reflects the depletion of ER stores and not the Ca^{2+} influx across the plasma membrane, since after ionomycin treatment the magnitude of the Ca^{2+} transients were essentially unchanged

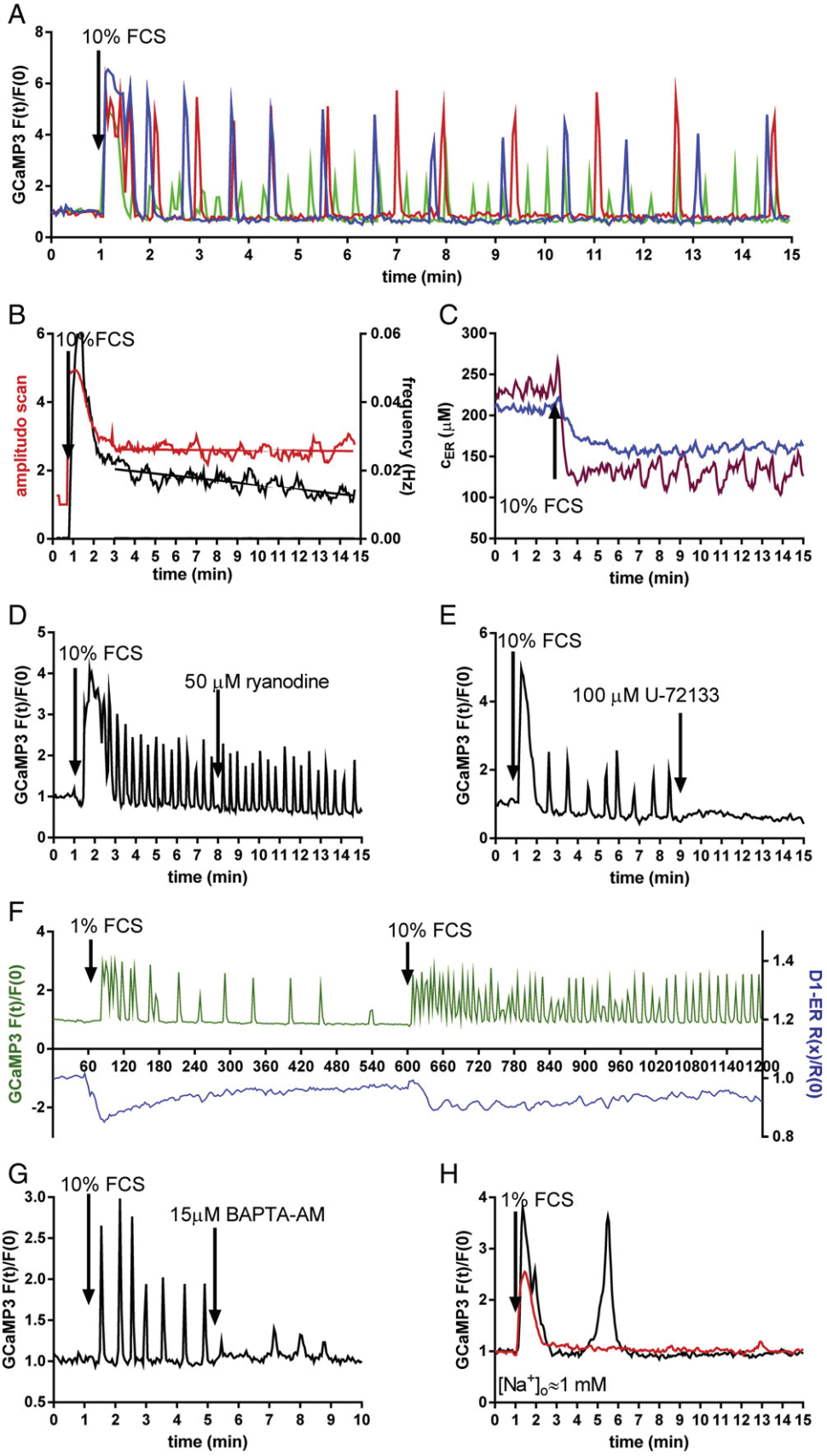

when the experiment was carried out at very low (<1 μM) external Ca^{2+} (Fig. 4A, red and green traces). The surface area of ER compartments is approximately 25–50 times larger (based on the data presented by Schmucker et al. [64]) than the surface of the plasma membrane; therefore the ionomycin-evoked Ca^{2+} leakage from the ER is more pronounced compared to the leakage through the plasma membrane. SERCA activity can't compensate for the elevated leakage from the ER and consequently the ER remained in a depleted state (Fig. 4A, blue trace). However, c_{cyt} recovered to near resting values, because the plasmalemmal extrusion system is able to cope with the increased Ca^{2+} influx. Although the ER was in a depleted state, the re-administration of serum after ionomycin treatment (500 nM) evoked an additional Ca^{2+} transient, indicative of the activation of ER load-independent serum-activated plasmalemmal Ca^{2+} channels (Fig. 4A, red trace). To test whether store-operated (SOC) i.e. ER load-dependent Ca^{2+} entry was also occurring in prMC, we employed THAPS, which causes passive Ca^{2+} emptying of ER stores that is expected to activate SOC-mediated Ca^{2+} entry. Cells were initially incubated in a Ca^{2+}-free solution; THAPS (5 μM) induced a slow increase in c_{cyt} marking the depletion of the ER stores. Increasing $[Ca^{2+}]_o$ to 1 mM resulted in a second increase of c_{cyt} most probably mediated via SOC entry (Fig. 4B red trace). In the absence of THAPS, an increase in $[Ca^{2+}]_o$ to 1 mM caused a minute, but prolonged increase in c_{cyt} (Fig. 4B black trace).

In the absence of extracellular Ca^{2+} ($[Ca^{2+}]_o \approx 0$ mM), ionomycin (50 nM) evoked a rise in c_{cyt} from basal levels to 350–400 nM (data not shown) together with an 80–90% depletion of luminal Ca^{2+} in the ER [65]. Using Eq. (6) we calculated a γ value of around 800–1300. Knowing that this equation somewhat overestimated γ, in our model we used a lower value, of $\gamma = 450$.

In the absence of extracellular Ca^{2+} (low Ca^{2+} solutions supplemented with 50 mM EGTA), prMC didn't show any Ca^{2+} response to 10% FCS administration in most cases. Only few cells displayed an initial small rise in c_{cyt}, without signs of Ca^{2+} oscillations (data not shown). In experiments, where the serum was added to Ca^{2+}-containing solutions $[Ca^{2+}]_o \approx 1$ mM and subsequently 10 mM EGTA was added to lower $[Ca^{2+}]_o$ to < 1 μM, the oscillations halted after one final Ca^{2+} spike (Fig. 4C). When EGTA (0.2 mM final) was added lowering $[Ca^{2+}]_o$ to ≈0.8 mM, a decrease in the oscillation frequency was observed (Fig. 4D). Contrarily, when $[Ca^{2+}]_o$ was raised from 1 mM to 2 mM, the oscillation frequency was increased (Fig. 4E). ML-9, an inhibitor of TRPC6 channels [66] that also inhibits myosin light chain kinase [67] and furthermore inhibits store-operated Ca^{2+} entry by inhibiting STIM1 recruitment [68] had a particular effect on the oscillations. ML-9 increased basal c_{cyt}, which resulted either in the stopping of the oscillations or in oscillations with a lower frequency, but with increased Ca^{2+} amplitudes and moreover, elevated basal c_{cyt} levels (Fig. 4F). Our results indicate that the main effect of ML-9, an inhibitor of limited specificity, was not the inhibition of the Ca^{2+} influx, but rather reducing the Ca^{2+} efflux rate, based on the slightly elevated basal c_{cyt} after ML-9 administration (Fig. 4F). SKF 96365 (100 μM), a compound that blocks both SOCs and DAG-activated TRPC channels [66,69] reducing the Ca^{2+} influx across the plasma membrane [70], either completely blocked (Fig. 4G, black trace) or strongly decreased the oscillation frequency. In conditions, when oscillations were not blocked, the amplitude of the Ca^{2+} signals was not affected (Fig. 4G, red trace). Interestingly, immediately after SKF 96365 administration, the drug evoked a brief Ca^{2+} transient in each cell, which either halted oscillations or resulted in frequency-reduced Ca^{2+} oscillations. Our model recapitulated the effect of SKF 96365 on Ca^{2+} oscillation and revealed that the oscillation frequency depended on the magnitude of Ca^{2+} influx. Decreasing the Ca^{2+} influx through plasma membrane Ca^{2+} channels decreased the frequency of Ca^{2+} oscillations (Fig. 4H, red trace). Completely switching off the influx ($J_{IN} = 0$) resulted in a stop of the oscillations (Fig. 4H, black trace).

3.4. Effect of blocking SERCA pumps on the oscillation frequency

While thapsigargin administered at high concentration (≥2 μM) completely blocked the Ca^{2+} oscillations, at lower concentrations, it modified the oscillation frequency in both directions, i.e. increasing it in some cells and lowering it in others (Fig. 5A). Both situations could be modeled by changing the parameter r_{s2} from 22 nM/s to 26.5 nM/s (Fig. 5B, C). The direction of the change caused by partial blocking of SERCA pumps was dependent on $[InsP_3]$. At lower concentration ($[InsP_3] = 0.18$ μM), the oscillation frequency was increased (Fig. 5B), while at higher concentrations ($[InsP_3] = 5$ μM) the oscillation frequency was decreased (Fig. 5C). Of note, the partial block of SERCA pumps resulted in an increase of basal c_{cyt} both in the model and in the experimental measurements.

3.5. Applying the model to experiments done by others

We simulated the effect of a transient brief $[InsP_3]$ increase ("$InsP_3$ step") on baseline spiking oscillations as previously measured in HEK293 cells (see Fig. 2B in [71]). $[InsP_3]$ was held constant except for a 30 s-theoretical $InsP_3$ step characterized by an immediate on/off step. During the baseline spiking oscillations, this instantaneous increase caused an immediate spike and a delay selectively of the next Ca^{2+} transient with no changes in the oscillation frequency of the following spikes (Fig. 6A). When the $InsP_3$ step was applied during high-frequency oscillations, this caused an increase in oscillation frequency (see Fig. 2A in [71]). In our model, at high Ca^{2+} influx rates ($J_{IN} > 12$ nM/s), high $[InsP_3]$ (>5 μM) and a raise of $[InsP_3]$ to 50 μM, this caused a transient elevation of the Ca^{2+} spike amplitude and increased the oscillation frequency during the period of elevated $[InsP_3]$ (Fig. 6B). Previous studies have reported on a critical c_{cyt} for spike development (see Fig. 4A in [72]). Our model predicts that the Ca^{2+} spike generation is Ca^{2+}-influx-independent within a certain range of c_{cyt} values and for this, basal c_{cyt} was set to 90 nM. If the Ca^{2+} influx was switched off at $c_{cyt} = 95$ nM ($J_{IN} = 0$), then no Ca^{2+} spike developed (Fig. 6C, part a), however if the Ca^{2+} influx was blocked at $c_{cyt} > 100$ nM (parts b,c), the amount of intracellular Ca^{2+} was sufficient to cause ER-mediated Ca^{2+} release representing the major component of the Ca^{2+} spike (Fig. 6C). Furthermore, during Ca^{2+} oscillations, a slight delay between the time points of maximum of c_{cyt} and the minimum of c_{ER} had been observed (see Fig. 4C in [27]). Our model also showed this phenomenon.

Fig. 2. Ca^{2+} oscillations in mesothelial cells after serum re-administration A. Single-cell fluorescent recordings from time-lapse videos show Ca^{2+} oscillations after serum re-administration. Each color track represents a single cell. B. For the calculations of the frequency (black trace) and amplitude scans (red trace) after serum re-administration, 100 GCaMP3-expressing mesothelial cells were evaluated. For determining the slopes, the time period from 2 min after serum addition until 13 min was considered. While the amplitude slope is not significantly different from zero ($p > 0.05$), the frequency decreases with time after serum addition ($p < 0.0001$). C. Two representative recordings from a D1ER-expressing cell show a rapid decrease in c_{ER} resulting from serum re-administration followed by a sawtooth wave in c_{ER}. D. A single-cell fluorescent recording from time-lapse videos shows Ca^{2+} oscillations after serum re-administration. Frequency and amplitude of the oscillation remained unchanged after administration of ryanodine (50 μM). E. A representative recording from a GCaMP3-expressing cell shows an oscillation arrest after administration of U-73122, a phospholipase C inhibitor. F. A representative recording from a GCaMP3-expressing mesothelial cell shows an increase in oscillation frequency after elevating the serum concentration from 1% (left) to 10% (right). Under the same conditions, c_{ER} was determined by D1ER in another mesothelial cell. At the lower serum concentration, c_{ER} nearly recovered from its semi-depleted state 10 min after serum (1%) addition, while it remained in a semi-depleted state when exposed to 10% serum. G. A representative single-cell fluorescent recording shows Ca^{2+} oscillations after serum re-administration. Administration of BAPTA-AM (15 μM) to the medium results in oscillations with lower amplitudes, but increased half-width of Ca^{2+} transients. H. In the absence of extracellular Na^+ ions ($[Na^+]_o \approx 1$ mM), in most cases only the initial Ca^{2+} spike is observed (red trace). In few cells, additional Ca^{2+} transients are detected (black trace). Two representative single-cell fluorescent recordings were selected.

The five phases of one oscillatory cycle are depicted in Fig. 6D and more details are provided in Table 2.

4 . Discussion

Oscillatory changes in c_{cyt} occur in excitable, as well as in non-excitable cells, including hepatocytes [73], embryonic intestinal epithelial cells [74] and pancreatic acinar cells [75]. The reason for not having observed Ca^{2+} oscillations in mesothelial cells before might be manifold: measurement of global Ca^{2+} signals (cuvette recordings) [3–6] vs. recordings in individual cells, the use of non-optimized Ca^{2+} indicator dyes with respect to K_D, k_{on} or high indicator concentrations, which were shown to modify Ca^{2+} oscillations [76,77]. Based on the large diversity of Ca^{2+} oscillation patterns in various cell types and moreover even within an apparently homogenous cell population [76], many different models were developed to describe these oscillations [78]. Despite the large number of studies reporting on the underlying processes leading to Ca^{2+} oscillations, no broad general consensus has been reached yet; however the various oscillation models can be classified into subgroups [79]. Our model is a channel-based, deterministic, open-cell model. With the modeling, we aimed to demonstrate how the measured dependent variables (c_{cyt} and c_{ER}) vary as the result of changes of the independent variables J_{IN} and [$InsP_3$].

As $InsP_3Rs$ are biphasically regulated by c_{cyt} [80], the $InsP_3R$-based models usually assume that $InsP_3Rs$ are quickly activated, but slowly inactivated by Ca^{2+} [81]. Consequently the period length of Ca^{2+} oscillations depends on the time required for $InsP_3R$ to recover from Ca^{2+}-induced inhibition. Thus, these models mostly fail to explain why the frequency of Ca^{2+} oscillations even in a single cell can vary in a very wide temporal range [79]. Other theories based on the function of putative $InsP_3R$ inhibitors [17,82] are faced with the same problem. If such an inhibitor inactivates the receptor at high c_{cyt}, then the next activation at low c_{cyt} will be governed by the K_D of the putative inhibitor. For instance, calmodulin was reported to inhibit $InsP_3R$ at elevated c_{cyt} [82], however this doesn't play a direct role in the biphasic modulation of $InsP_3R$ by c_{cyt} [83].

We solved this problem by taking into account the regulatory effect of c_{ER} on $InsP_3R$. High c_{ER} increases the open probability rate of $InsP_3R$; low c_{ER} decreases the open probability [84–86]. The "store loading Ca^{2+} oscillatory" theory [17,46] takes into account the $InsP_3R$ regulation by c_{ER}. After a Ca^{2+} spike, c_{ER} is decreased and has to recover before $InsP_3Rs$ are resensitized to deliver the next Ca^{2+} pulse. Thus, the interspike interval is essentially determined by the velocity of ER loading. Although this theory allows for a constant c_{cyt} and an increasing c_{ER} during interspike periods [4], the mathematical model based on this theory does not show this phenomenon [87]. Because our experimental data confirmed that in mesothelial cells a sawtooth wave in c_{ER} is paralleled by a baseline spiking oscillation in c_{cyt}, we integrated the "store loading Ca^{2+} oscillatory" concept into our model. The sawtooth wave in c_{ER} was also found in BHK-21 fibroblast cells after bradykinin stimulation [88].

In our simulations a Ca^{2+} spike starts with a small elevation in c_{cyt}, and with a little delay c_{ER} reaches its maximum before it starts to decrease, i.e. the slow rise of c_{cyt} (foot) precedes the decrease of c_{ER} (Fig. 6D), as was also proven experimentally [89]. The foot period of the spike (Fig. 6D) lasts until a critical level $c_{cyt,crit}$ is reached. At c_{cyt} lower than the $c_{cyt,crit}$ value, the spike development is based on Ca^{2+} influx, but the further development of the spike is influx-independent, i.e. the activation of $InsP_3R$ is mediated exclusively by the increased c_{cyt}. This self-sustaining phenomenon is called "Ca^{2+}-induced Ca^{2+} release"

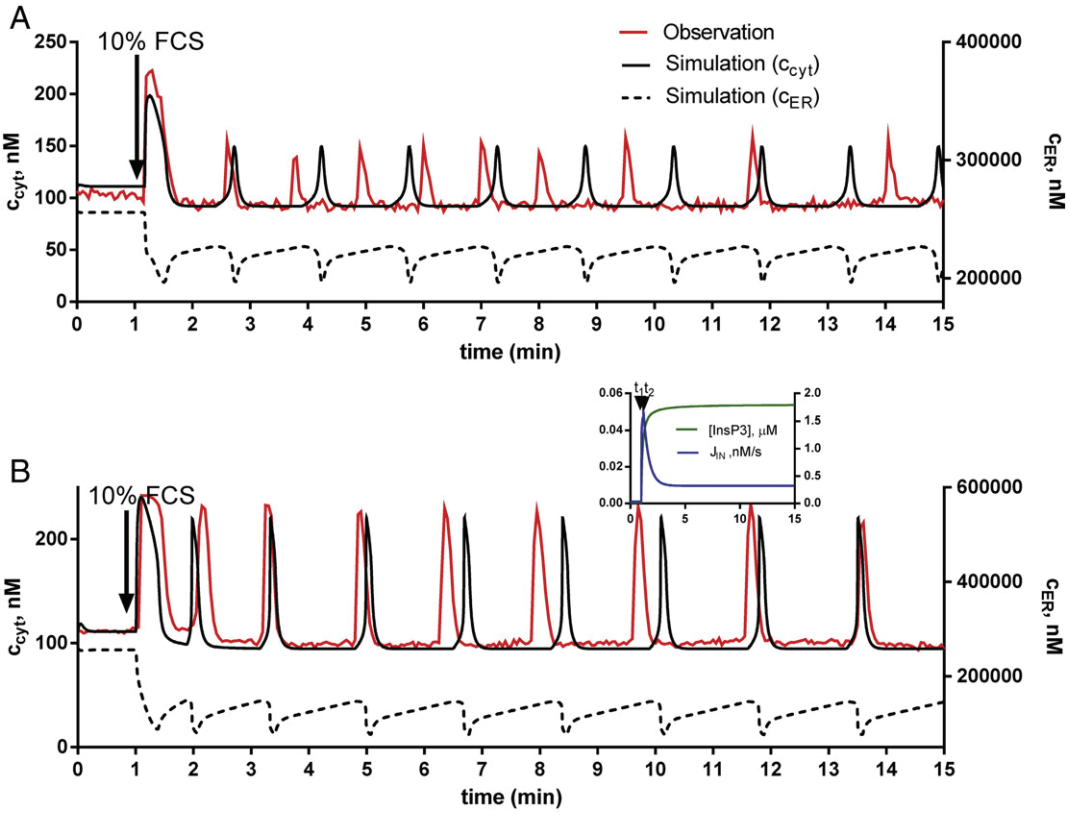

Fig. 3. Modeling of serum-induced Ca^{2+} oscillations. A. A mesothelial cell recording (red trace) showing low [$InsP_3$]-based oscillations was selected for the fitting. The parameters for J_{IN} and [$InsP_3$] are: $t_1 = 70$ s, $t_2 = 75$ s, $r_{IN,MAX} = 5$ nM/s, $r_{IN,p} = 0.35$ nM/s, $K_{IN,1} = 0.005$, $K_{IN,2} = 10$, $i_{IP3,MAX} = 0.24$ µM, $K_{IP3} = 0.01$. For the modeling, the initial c_{ER} was set at 257 µM, resulting in a slightly lower resting c_{cyt} than in the standard simulations, where c_{ER} was set at 260 µM. The simulations for c_{cyt} (black solid line) and for c_{ER} (black dashed line) result in a pattern closely resembling the one of c_{cyt} obtained from the experimental recording. B. A recording showing high [$InsP_3$]-based oscillations (red trace) was selected for the model fitting. Black lines (solid and dashed) represent the modeled c_{cyt} and c_{ER}, respectively. The small insert represents the changes in independent parameters for the Ca^{2+} influx and [$InsP_3$]: $t_1 = 60$ s, $t_2 = 72$ s, $r_{IN,MAX} = 5$ nM/s, $r_{IN,p} = 1.05$ nM/s, $K_{IN,1} = 0.01$, $K_{IN,2} = 2$, $i_{IP3,MAX} = 1.8$ µM, $K_{IP3} = 0.1$. Note the close match between the modeled and measured traces.

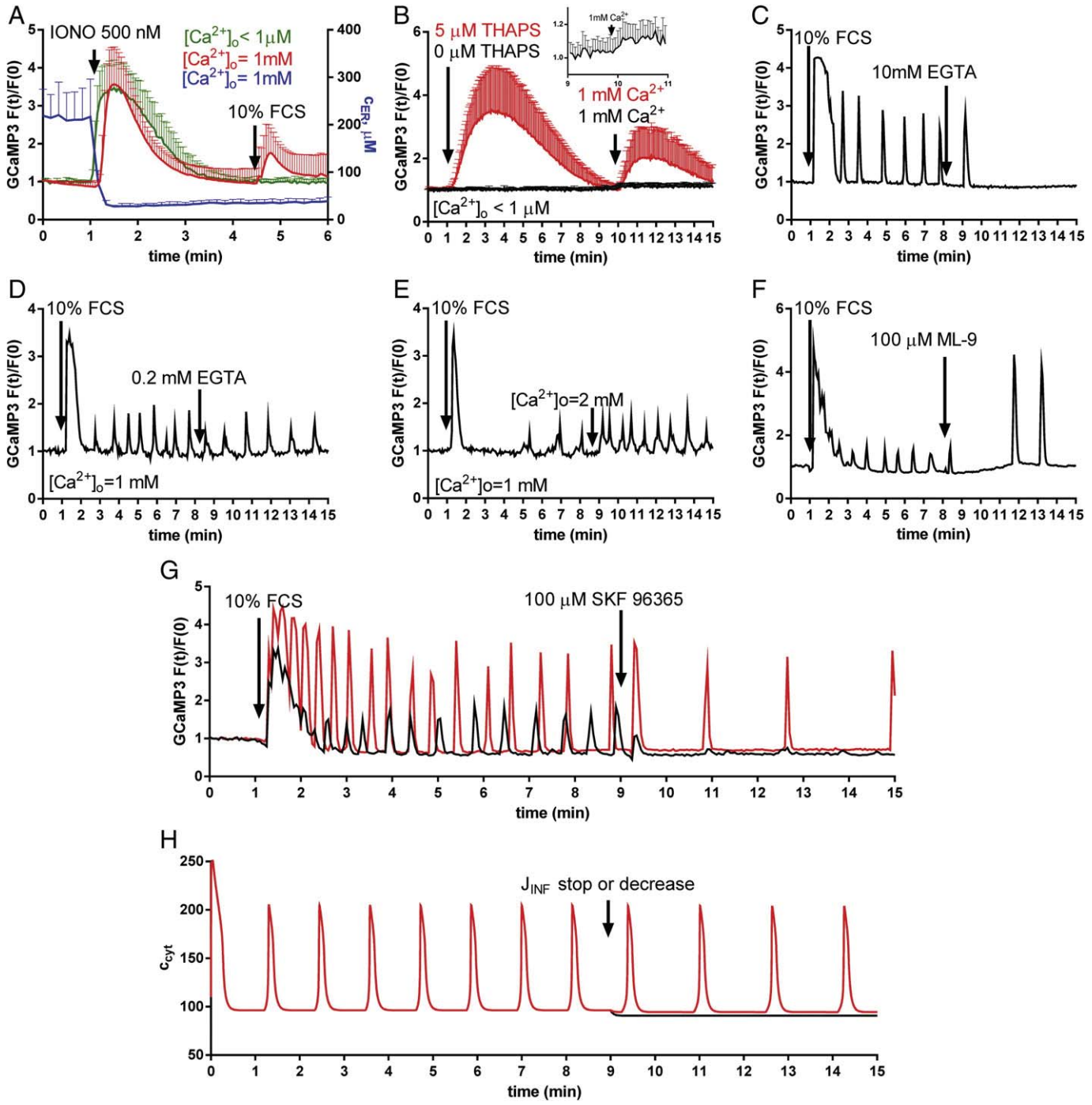

Fig. 4. Characterization of Ca^{2+} influx across the plasma membrane. A. Ionomycin (500 nM) depletes ER Ca^{2+} stores (blue trace) and evokes a rapid increase in c_{cyt}, followed by a Ca^{2+} decay phase not completely returning to basal c_{cyt} values; both, in the presence (red trace) and absence (green trace) of extracellular Ca^{2+}. Re-administration of serum at a time point when the ionomycin-induced Ca^{2+} transient is close to basal c_{cyt}, leads to a transient in c_{cyt} likely via ER load-independent influx components only in the presence of extracellular Ca^{2+} (red trace). The curves are averages from 10 cells (mean ± SD). B. In the absence of extracellular Ca^{2+} ($[Ca^{2+}]_o$ < 1 μM), thapsigargin (5 μM) evokes a Ca^{2+} signal. Increasing $[Ca^{2+}]_o$ to 1 mM leads to an additional rise in c_{cyt} mediated by SOC channels evidenced in GCaMP3-expressing mesothelial cells (red trace). In the absence of thapsigargin, an increase in $[Ca^{2+}]_o$ causes a minute, but prolonged increase in c_{cyt} (black trace and inset). The curves are averages from 10 cells (mean ± SD). C–E. Representative single-cell fluorescent recordings from time-lapse videos shows Ca^{2+} oscillations after serum re-administration; C. extracellular Ca^{2+} removal by the addition of EGTA (10 mM) results in one final Ca^{2+} spike before cessation of oscillations; D. a decrease in $[Ca^{2+}]_o$ from 1 mM to approximately 0.8 mM by administration of 0.2 mM EGTA results in a decreased oscillation frequency; E. increasing $[Ca^{2+}]_o$ to 2 mM leads to an increase in oscillation frequency. F. A representative single-cell fluorescent recording shows Ca^{2+} oscillations after serum re-administration. ML-9 slowly increases basal c_{cyt}, which results in oscillations with a lower frequency, but increased Ca^{2+} amplitudes. G. The frequency of serum-induced Ca^{2+} oscillations is blocked (black trace) or attenuated (red trace) by administration of 100 μM SKF 96365, yet the amplitudes remain unchanged. H. Model-based simulation. The independent variables are: $[InsP_3] = 1$ μM, constant from $t_0 \rightarrow t_{end}$ and $J_{IN} = 15$ nM/s, ($t_0 \rightarrow t_{9\ min}$), $J_{IN} = 1$ nM/s ($t_{9\ min} \rightarrow t_{end}$) (red trace) and $J_{IN} = 0$ nM/s ($t_{9\ min} \rightarrow t_{end}$) (black trace). The frequency of serum-induced Ca^{2+} oscillation is attenuated by partially blocking the Ca^{2+} influx, yet the amplitudes remain essentially unchanged. A complete block of Ca^{2+} influx stops the oscillations (black trace).

[90]. As reported before [72], Ca^{2+} entry is necessary for sustained oscillatory activity, but its contribution and thus importance changes during the rising phase of a Ca^{2+} spike: the slow rise in c_{cyt} at the beginning requires Ca^{2+} entry, but the rapid upstroke phase doesn't. Our model also highlights that the maximum of c_{cyt} precedes the minimum of c_{ER}, similar to what was found by Shmigol et al. [91], Dagnino-Acosta

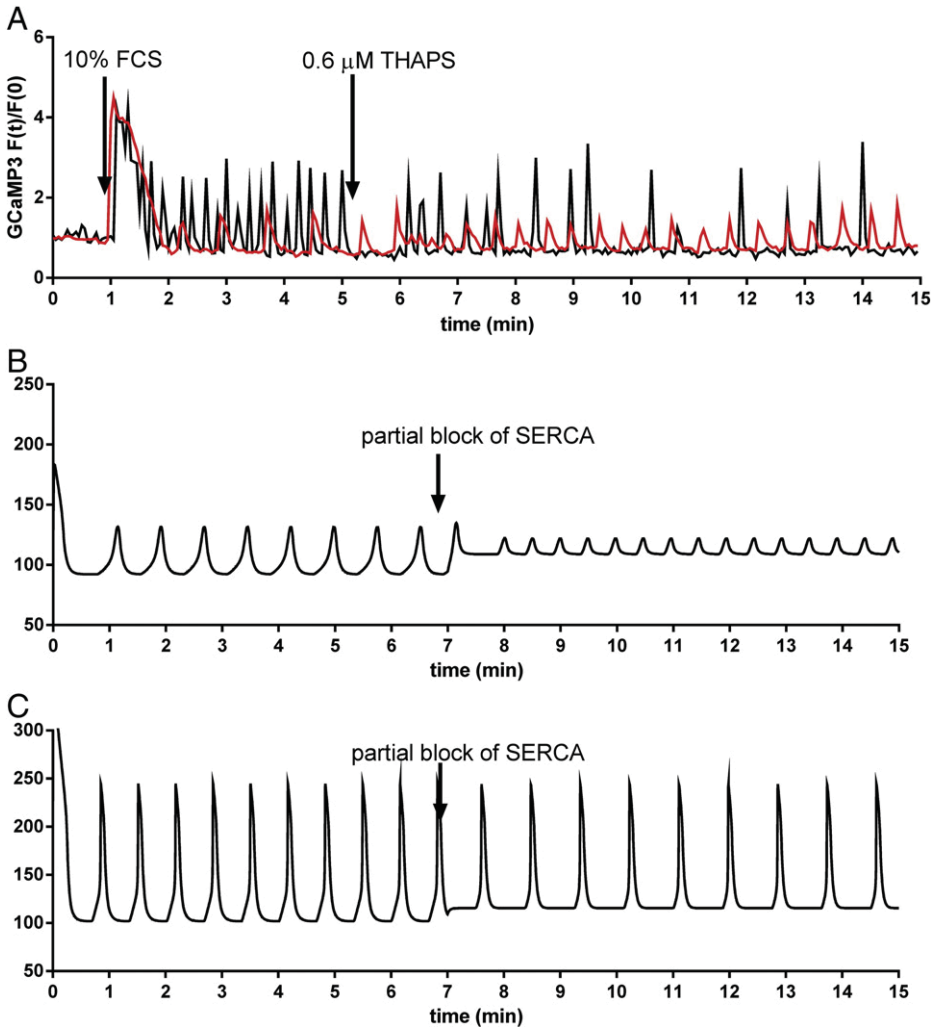

Fig. 5. Modeling the effect of a partial block of SERCA pumps on Ca^{2+} oscillations. A. Partial blocking of SERCA pumps by thapsigargin (THAPS) modifies the frequency of the oscillation in both directions. In one case, the partial block of SERCA activity results in an increase in oscillation frequency (red trace), while in another cell, THAPS decreases the oscillation frequency (black trace). B. The oscillation frequency is increased, when the parameter r_{S2} is changed from 22 nM/s to 26.5 nM/s at $t = 7$ min. Independent parameters are: $J_{IN} = 0.4$ nM/s ($t_0 \rightarrow t_{end}$), $[InsP_3] = 0.18$ μM ($t_0 \rightarrow t_{end}$) C. Oscillation frequency is decreased when the parameter r_{S2} (SERCA activity) is changed from 22 nM/s to 26.5 nM/s at $t = 7$ min. Independent parameters are: $J_{IN} = 3$ nM/s ($t_0 \rightarrow t_{end}$), $[InsP_3] = 5$ μM ($t_0 \rightarrow t_{end}$). Note that in both cases basal c_{cyt} is increased after partial block of SERCA pumps.

and Guerrero-Hernández [92], Palmer et al. [27] and Ishii et al [89], all of whom reported a slight delay between the maximum of c_{cyt} and the minimum of c_{ER}. The changes of the different parameters during the five phases of an oscillation are summarized in Fig. 6D and in Table 2.

According to our model, the frequency of the baseline spiking oscillations depends on (I) the Ca^{2+} influx; the stronger the Ca^{2+} influx, the higher the frequency. This is in line with previous findings that an increase in extracellular Ca^{2+} during serotonin-induced oscillations in bowfly salivary glands accelerates Ca^{2+} oscillations without increasing $[InsP_3]$ [93]. It further depends on (II) the amount of Ca^{2+} that is removed from the cell during one Ca^{2+} spike (the larger the Ca^{2+} removal, the slower the oscillation) and (III) the rate of change in $[InsP_3]$ (the faster the rate of $InsP_3$ production, the faster the oscillation). Of interest, the mere rise in $[InsP_3]$ without Ca^{2+} influx ($J_{IN} = 0$) leads to few oscillations that stop once the elevated steady-state $[InsP_3]$ is reached. At a constant $[InsP_3]$ the oscillation frequency is then determined and maintained by IN and EFF processes. Tanimura and Turner [50] demonstrated $InsP_3$-dependent Ca^{2+} oscillations within the lumen of the ER of saponin-permeabilized HSY cells by monitoring c_{ER} with the fluorescent Ca^{2+} indicator Mag-fura-2. HSY cells exposed to successively higher concentrations of $InsP_3$ show few oscillations in c_{ER} when $[InsP_3]$ is increased from 0.3 to 0.6 μM. Then, c_{ER} remains constant and moreover, lower than before the increase in $[InsP_3]$ and consequently, no oscillations are observed afterwards. However, c_{ER} oscillations reappear after an additional increase in $[InsP_3]$ to 1 or 3 μM and moreover, the rate of decrease in c_{ER} (slope) is higher at higher $[InsP_3]$ and this is also paralleled by a higher oscillation frequency (for details, see Fig. 1 in [50]). Of note in intact cells this effect is masked by two additional factors. The higher $[InsP_3]$ causes a larger ER depletion, which due to the activation of SOC channels results in a stronger Ca^{2+} influx, and consequently increased oscillation frequency. On the other hand, the increased $[InsP_3]$ produces higher peaks in c_{cyt}, i.e. the amount of Ca^{2+} ions that are removed by plasmalemmal pumps is also increased. This in turn, slows down the frequency. In the experiments carried out at lower serum concentration (1%; Fig. 2F) expected to lead to weaker cell activation, the oscillation frequency (after the fast oscillation period of approximately 120 s) was clearly lower and accompanied with a faster recovery of c_{ER} from its semi-depleted state. Since the c_{ER} depletion level is highly correlated with $[InsP_3]$, we assume a time-dependent decrease in the rate of $InsP_3$ production during 1% FCS-induced oscillations. On the other hand, the stronger 10% FCS-induced cell activation leads to higher frequency oscillations, a nearly constant, semi-depleted ER state during the oscillations and presumably to constant $[InsP_3]$ levels. Thus, the model reveals that both, a decreased

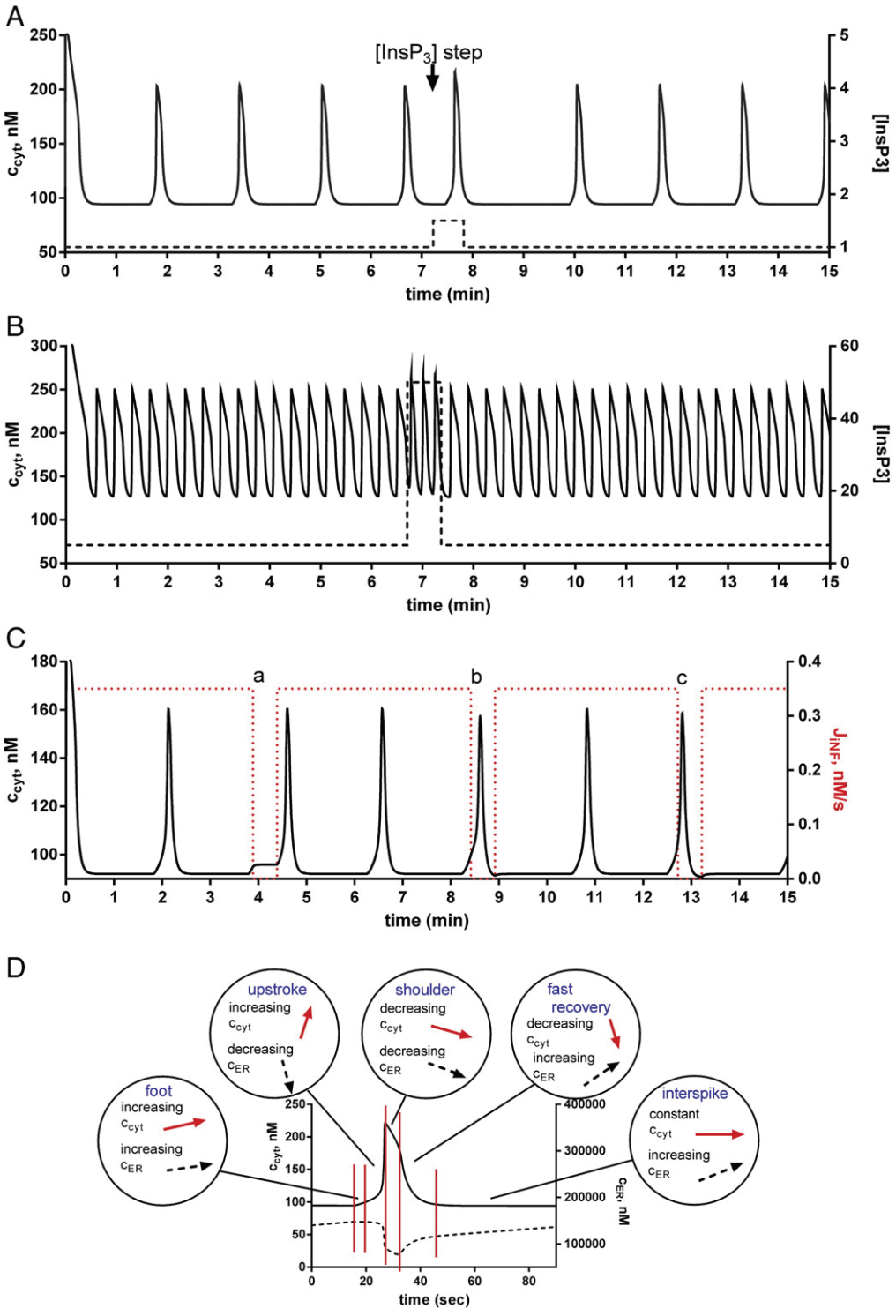

Fig. 6. Model simulations based on experiments previously reported by others. A. In an oscillating airway smooth muscle cell, an instantaneous, flash photolysis-induced increase in [$InsP_3$] results in an initial Ca^{2+} spike and a delay of only the next peak of the Ca^{2+} oscillation without changing the oscillation frequency [71]. Our model simulation demonstrates the effect of a rapid transient [$InsP_3$] increase during slow baseline spiking oscillations applied just before the onset of the "regular" spiking. This results in an immediate Ca^{2+} spike and a delay of the next Ca^{2+} spike, without globally affecting the oscillation frequency. The independent variables are: $J_{IN} = 1$ nM/s ($t_0 \rightarrow t_{end}$), changes in [$InsP_3$] are shown at the bottom of the x-axis. B. In an oscillating pancreatic acinar cell, the photorelease of $InsP_3$ causes a transient increase in oscillation frequency [71]. In our model when the duration of the transient elevation of [$InsP_3$] is longer than one oscillatory cycle, a transient elevation of [$InsP_3$] from 5 to 50 mM (dashed line) causes a transient increase in the oscillation frequency and in the maximal amplitude c_{cyt}, evident only during the increased $InsP_3$ step. The independent variable is: $J_{IN} = 12$ nM/s ($t_0 \rightarrow t_{end}$). C. The existence of a critical c_{cyt} concentration for spike development was proven in sympathetic neurons [72]. Our model shows that during the spike development the initial small rise in c_{cyt} depends on extracellular Ca^{2+} influx, the following fast rise is caused by ER depletion and is independent of Ca^{2+} influx. The independent variables are: [$InsP_3$] = 0.3 μM ($t_0 \rightarrow t_{end}$), the changes in J_{IN} are shown by the dashed line. If J_{IN} is switched off at c_{cyt} = 95 nM (*a*), the Ca^{2+} spike development is halted. If J_{IN} is switched off at c_{cyt} = 100 nM (*b*) or c_{cyt} = 105 nM (*c*), a regular full-size Ca^{2+} spike develops. D. Details on the kinetics of Ca^{2+} spike development (see also Table 2).

Ca^{2+} influx and a decreasing rate of $InsP_3$ production are likely to be the cause for the decreased oscillation frequency observed at the lower serum concentration.

The partial block of SERCA pumps may affect the oscillations frequencies in both directions. In the same cell culture dish, application of thapsigargin caused an increase in oscillation frequency in some cells, while decreasing it in others (Fig. 5). This phenomenon is also observable in recordings from oscillating pancreatic cells (decreasing frequency in [94], increasing frequency in [36]). Our model revealed that thapsigargin decreases the frequencies at higher spike amplitudes, when oscillations are most probably the result of higher [$InsP_3$] (Fig. 5B) and accelerates it at lower amplitudes during low [$InsP_3$]-based oscillations (Fig. 5C). Previous experimental data also showed that oscillations at semi-depleted c_{ER} states reflecting the increased [$InsP_3$] cause the increased amplitudes in c_{cyt} [95].

In our model, the plasmalemmal Ca^{2+} influx (J_{IN}) and [$InsP_3$] are the independent parameters; changing these parameters in time leads to Ca^{2+} oscillations ranging from fast, nearly sinusoidal to slow baseline spiking oscillations, i.e. the interspike period may vary from <10 s to extended time periods, i.e. to a stop of the oscillations. For faster, overlapping or irregular oscillations it might be necessary to expand our model in space and taking into account that the synchronization between the individual oscillatory units might be lost at higher frequencies. The Ca^{2+} influx (J_{IN}) was modeled with Michaelis–Menten kinetics and an exponential decay ending on a plateau (peak-plateau shape) (inset in Fig. 3B). Experimentally we found that J_{IN} contains also a SOC-independent i.e. an ER load-independent component (Fig. 4A). In our simulation, the ER load-independent Ca^{2+} influx results in the brief maximal influx rate, while the ER load-dependent SOC entry is responsible for the plateau phase of J_{IN} (inset in Fig. 3B).

The change in [$InsP_3$] was simulated as a rapid increase quickly leveling off. Kinetics of [$InsP_3$] changes measured with a specific indicator protein showed Michaelis–Menten kinetics upon stimulation with endothelin-1 [96] in rat oocytes. Matsu-ura et al. [97] also found that [$InsP_3$] gradually accumulated in the cytosol with little or no fluctuations during Ca^{2+} oscillations. Experimentally observed small fluctuations in [$InsP_3$] are considered as passive reflections of the Ca^{2+} oscillations (increased PLC activity and $InsP_3$ production during peak c_{cyt}) and not essential for the driving of the Ca^{2+} oscillations [54].

Sneyd et al. [71] reported that pulmonar acinar cells show carbachol-induced Ca^{2+} oscillations. An instantaneous, flash photolysis-induced increase in [$InsP_3$] during ongoing oscillations results in a delay before the spike without a change in oscillation frequency. However, a similar increase in [$InsP_3$] causes a transient increase in oscillation frequency in airway smooth muscle cells. The authors thus proposed different underlying mechanisms and thus different models for Ca^{2+} oscillations present in these two cell types. Our model can recapitulate both phenomena: an $InsP_3$ step during baseline spiking oscillations leads to a delay of the next spike (Fig. 6A), while a similar step during fast oscillations increases the oscillation frequency during the step duration (Fig. 6B), i.e. the effects are $InsP_3R$-based in both cases.

Although we didn't incorporate mitochondria in our model, these organelles influence Ca^{2+} oscillations in two ways. First, mitochondria produce ATP, required for SERCA and PMCA functions. Second, the Ca^{2+} concentrations in the matrix of the mitochondria also change and slightly oscillate during cytoplasmic Ca^{2+} oscillations [89]. In regard to our model, the mitochondria act in a similar way as the extracellular space. During the spikes, Ca^{2+} ions move from the cytoplasm into the mitochondrial matrix and during the interspike intervals Ca^{2+} ions are transported from the mitochondrial matrix to the cytoplasm. In some cell types, the matrix volume and their Ca^{2+} storing capacity might be so effective as to maintain the Ca^{2+} oscillations even in absence of extracellular Ca^{2+} [89] or by blocking IN and EFF by lanthanide [98]. In mesothelial cells, however, mitochondrial Ca^{2+} uptake appears to play a marginal role in Ca^{2+} oscillations. Removal of extracellular Ca^{2+} ions by EGTA chelation causes an arrest in Ca^{2+} oscillations and Ru360, a blocker of mitochondrial Ca^{2+} uniporter (MCU), didn't stop these oscillations. Nevertheless, further experiments need to be performed to decipher the exact role of mitochondria in Ca^{2+} oscillations.

Conflict of interest statement

(1) We have included in the Acknowledgement all third-party financial support for the work in the submitted manuscript.
(2) All financial relationships with any entities that could be viewed as relevant to the general area of the submitted manuscript have been added in the Acknowledgement.
(3) This includes all sources of revenue with relevance to the submitted work, who made payments to us, or our institution on your behalf, in the 36 months prior to submission.
(4) There are no interactions with sponsors outside of the submitted work.
(5) There are no relevant patents or copyrights (planned, pending, or issued) resulting from this work.
(6) There are no other relationships or affiliations that may be perceived by readers to have influenced, or give the appearance of potentially influencing, what you wrote in the submitted work.

Acknowledgements

The authors are grateful to Walter Blum, Anatomy, Dept. of Medicine, University of Fribourg for assistance during isolation of primary

Table 2
Five phases of one cycle of baseline spiking Ca^{2+} oscillations.

	Interspike	Rising phase		Decay phase	
		Foot	Upstroke	Shoulder	Fast recovery
c_{cyt}	Constant	Increasing	Increasing	Decreasing	Decreasing
c_{ER}	Increasing	Increasing	Decreasing	Decreasing	Increasing
Duration-determining parameter	J_{IN}	J_{IN}	J_{EREFF} (Ca^{2+}-induced Ca^{2+} release)	J_{EFF}	J_{SERCA}
$InsP_3R$ activity (J_{EREFF})	Zero	Increasing	Increasing	Decreasing	Zero
J_{IN}	Constant				
J_{EFF}	Low[a]	Low[a]	Low[a] and then increasing	Decreasing	Decreasing and then low[a]
J_{SERCA}	Constant	Increasing	Increasing	Decreasing	Decreasing
Activating effect of c_{cyt} on $InsP_3R$	Constant	Increasing	Increasing and then decreasing	Decreasing	Decreasing
Inhibitory effect of c_{ER} on $InsP_3R$	Decreasing	Decreasing	Increasing	Increasing and then decreasing	Decreasing
Phase starting at	Basal c_{cyt}	c_{ER}/c_{cyt} maximum	c_{ER} maximum "critical c_{cyt}"	c_{cyt} maximum	c_{ER} minimum
[$InsP_3$]	Constant				

[a] "Low" denotes zero or a value that is smaller than the value of J_{IN}.

mouse mesothelial cells and to Scott A. Thomson, Dept. of Mathematics, University of Fribourg, for verifying the mathematical equations. The authors would like to thank Michael J. Berridge, Babraham Institute, Cambridge, Hartmut Schmidt, University of Leipzig, Thomas Henzi and Walter Blum, University of Fribourg, for helpful discussion and careful reading of the manuscript. The authors thank Dr. D. Trono (EPFL, Lausanne, Switzerland) for providing pLVTHM (Addgene plasmid #12247), pMD2G-VSVG (Addgene plasmid #12259) and pCMV-dR8.91, Dr. L. Looger for GCaMP3 (Addgene plasmid #22692), Dr. R. E. Campbell for GEM-GECO1 (Addgene Plasmid #32442) and Dr. R. Y. Tsien for D1ER (Addgene #36325). The work was partially supported by an SNF grant to B.S. (#130680).

Appendix A. Supplementary data

Supplementary data to this article can be found online

References

[1] S.E. Mutsaers, The mesothelial cell, Int. J. Biochem. Cell Biol. 36 (2004) 9–16.
[2] S. Yung, T.M. Chan, Mesothelial cells, Perit. Dial. Int. 27 (Suppl. 2) (2007) S110–S115.
[3] S.D. Bird, R.J. Walker, Effects of bicarbonate buffered dialysate on human peritoneal mesothelial cell intracellular calcium homeostasis, Nephrology (Carlton) 8 (2003) 150–155.
[4] S.D. Bird, R.J. Walker, Mast cell histamine-induced calcium transients in cultured human peritoneal mesothelial cells, Perit. Dial. Int. 18 (1998) 626–636.
[5] K. Ito, M. Kuwahara, S. Sugano, Role of intra- and extracellular calcium stores in mesothelial cell response to histamine, Am. J. Physiol. 268 (1995) L63–L70.
[6] S.D. Bird, Q. Hasan, P.F. Davis, R.J. Walker, Platelet derived growth factor-BB induced calcium transients in cultured human peritoneal mesothelial cells, ASAIO J. 44 (1998) 835–840.
[7] T.H. Cheung, T.A. Rando, Molecular regulation of stem cell quiescence, Nature reviews, Mol. Cell Biol. 14 (2013) 329–340.
[8] M.A. Foreman, J. Smith, S.J. Publicover, Characterisation of serum-induced intracellular Ca2+ oscillations in primary bone marrow stromal cells, J. Cell. Physiol. 206 (2006) 664–671.
[9] A. Wood, M.G. Wing, C.D. Benham, D.A. Compston, Specific induction of intracellular calcium oscillations by complement membrane attack on oligodendroglia, J. Neurosci. 13 (1993) 3319–3332.
[10] M.J. Berridge, Calcium oscillations, J. Biol. Chem. 265 (1990) 9583–9586.
[11] A.S. Goustin, E.B. Leof, G.D. Shipley, H.L. Moses, Growth factors and cancer, Cancer Res. 46 (1986) 1015–1029.
[12] E. Rozengurt, Early signals in the mitogenic response, Science 234 (1986) 161–166.
[13] J.B. Morris, K.A. Hinchliffe, A. Ciruela, A.J. Letcher, R.F. Irvine, Thrombin stimulation of platelets causes an increase in phosphatidylinositol 5-phosphate revealed by mass assay, FEBS Lett. 475 (2000) 57–60.
[14] T.R. Hesketh, J.D. Morris, J.P. Moore, J.C. Metcalfe, Ca2+ and pH responses to sequential additions of mitogens in single 3T3 fibroblasts: correlations with DNA synthesis, J. Biol. Chem. 263 (1988) 11879–11886.
[15] V. See, N.K. Rajala, D.G. Spiller, M.R. White, Calcium-dependent regulation of the cell cycle via a novel MAPK–NF-kappaB pathway in Swiss 3T3 cells, J. Cell Biol. 166 (2004) 661–672.
[16] B. Margolis, S.G. Rhee, S. Felder, M. Mervic, R. Lyall, A. Levitzki, A. Ullrich, A. Zilberstein, J. Schlessinger, EGF induces tyrosine phosphorylation of phospholipase C-II: a potential mechanism for EGF receptor signaling, Cell 57 (1989) 1101–1107.
[17] M.J. Berridge, Inositol trisphosphate and calcium signalling, Nature 361 (1993) 315–325.
[18] A. Dietrich, H. Kalwa, B.R. Rost, T. Gudermann, The diacylgylcerol-sensitive TRPC3/6/7 subfamily of cation channels: functional characterization and physiological relevance, Pflugers Arch. 451 (2005) 72–80.
[19] J.T. Smyth, S.Y. Hwang, T. Tomita, W.I. DeHaven, J.C. Mercer, J.W. Putney, Activation and regulation of store-operated calcium entry, J. Cell. Mol. Med. 14 (2010) 2337–2349.
[20] F. Moccia, R. Berra-Romani, S. Tritto, S. Signorelli, V. Taglietti, F. Tanzi, Epidermal growth factor induces intracellular Ca2+ oscillations in microvascular endothelial cells, J. Cell. Physiol. 194 (2003) 139–150.
[21] M. Morita, C. Higuchi, T. Moto, N. Kozuka, J. Susuki, R. Itofusa, J. Yamashita, Y. Kudo, Dual regulation of calcium oscillation in astrocytes by growth factors and pro-inflammatory cytokines via the mitogen-activated protein kinase cascade, J. Neurosci. 23 (2003) 10944–10952.
[22] R. Hu, M.L. He, H. Hu, B.X. Yuan, W.J. Zang, C.P. Lau, H.F. Tse, G.R. Li, Characterization of calcium signaling pathways in human preadipocytes, J. Cell. Physiol. 220 (2009) 765–770.
[23] J. Bot, D. Whitaker, J. Vivian, R. Lake, V. Yao, R. McCauley, Culturing mouse peritoneal mesothelial cells, Pathol. Res. Pract. 199 (2003) 341–344.
[24] N.D. Connell, J.G. Rheinwald, Regulation of the cytoskeleton in mesothelial cells: reversible loss of keratin and increase in vimentin during rapid growth in culture, Cell 34 (1983) 245–253.
[25] L. Tian, S.A. Hires, T. Mao, D. Huber, M.E. Chiappe, S.H. Chalasani, L. Petreanu, J. Akerboom, S.A. McKinney, E.R. Schreiter, C.I. Bargmann, V. Jayaraman, K. Svoboda, L.L. Looger, Imaging neural activity in worms, flies and mice with improved GCaMP calcium indicators, Nat. Methods 6 (2009) 875–881.
[26] Y. Zhao, S. Araki, J. Wu, T. Teramoto, Y.F. Chang, M. Nakano, A.S. Abdelfattah, M. Fujiwara, T. Ishihara, T. Nagai, R.E. Campbell, An expanded palette of genetically encoded Ca(2)(+) indicators, Science 333 (2011) 1888–1891.
[27] A.E. Palmer, C. Jin, J.C. Reed, R.Y. Tsien, Bcl-2-mediated alterations in endoplasmic reticulum Ca2+ analyzed with an improved genetically encoded fluorescent sensor, Proc. Natl. Acad. Sci. U. S. A. 101 (2004) 17404–17409.
[28] M. Wiznerowicz, D. Trono, Conditional suppression of cellular genes: lentivirus vector-mediated drug-inducible RNA interference, J. Virol. 77 (2003) 8957–8961.
[29] R.H. Kutner, X.Y. Zhang, J. Reiser, Production, concentration and titration of pseudotyped HIV-1-based lentiviral vectors, Nat. Protoc. 4 (2009) 495–505.
[30] R. Rudolf, P.J. Magalhaes, T. Pozzan, Direct in vivo monitoring of sarcoplasmic reticulum Ca2+ and cytosolic cAMP dynamics in mouse skeletal muscle, J. Cell Biol. 173 (2006) 187–193.
[31] A.G. Manford, C.J. Stefan, H.L. Yuan, J.A. Macgurn, S.D. Emr, ER-to-plasma membrane tethering proteins regulate cell signaling and ER morphology, Dev. Cell 23 (2012) 1129–1140.
[32] G. Dupont, A. Abou-Lovergne, L. Combettes, Stochastic aspects of oscillatory Ca2+ dynamics in hepatocytes, Biophys. J. 95 (2008) 2193–2202.
[33] N.F. al-Baldawi, R.F. Abercrombie, Calcium diffusion coefficient in Myxicola axoplasm, Cell Calcium 17 (1995) 422–430.
[34] R.C. Young, P. Zhang, The mechanism of propagation of intracellular calcium waves in cultured human uterine myocytes, Am. J. Obstet. Gynecol. 184 (2001) 1228–1234.
[35] E. Hernandez-SanMiguel, L. Vay, J. Santo-Domingo, C.D. Lobaton, A. Moreno, M. Montero, J. Alvarez, The mitochondrial Na+/Ca2+ exchanger plays a key role in the control of cytosolic Ca2+ oscillations, Cell Calcium 40 (2006) 53–61.
[36] L.E. Fridlyand, N. Tamarina, L.H. Philipson, Modeling of Ca2+ flux in pancreatic beta-cells: role of the plasma membrane and intracellular stores, Am. J. Physiol. Endocrinol. Metab. 285 (2003) E138–E154.
[37] A.J. Caride, A.R. Penheiter, A.G. Filoteo, Z. Bajzer, A. Enyedi, J.T. Penniston, The plasma membrane calcium pump displays memory of past calcium spikes. Differences between isoforms 2b and 4b, J. Biol. Chem. 276 (2001) 39797–39804.
[38] C.C. Fink, B. Slepchenko, I.I. Moraru, J. Watras, J.C. Schaff, L.M. Loew, An image-based model of calcium waves in differentiated neuroblastoma cells, Biophys. J. 79 (2000) 163–183.
[39] J. Herrington, Y.B. Park, D.F. Babcock, B. Hille, Dominant role of mitochondria in clearance of large Ca2+ loads from rat adrenal chromaffin cells, Neuron 16 (1996) 219–228.
[40] P.C. Chandrasekera, M.E. Kargacin, J.P. Deans, J. Lytton, Determination of apparent calcium affinity for endogenously expressed human sarco(endo)plasmic reticulum calcium-ATPase isoform SERCA3, Am. J. Physiol. Cell Physiol. 296 (2009) C1105–C1114.
[41] C.J. Favre, J. Schrenzel, J. Jacquet, D.P. Lew, K.H. Krause, Highly supralinear feedback inhibition of Ca2+ uptake by the Ca2+ load of intracellular stores, J. Biol. Chem. 271 (1996) 14925–14930.
[42] E.A. Turovsky, N.P. Kaimachnikov, M.V. Turovskaya, A.V. Berezhnov, V.V. Dynnik, V.P. Zinchenko, Two mechanisms of calcium oscillations in adipocytes, Biochem. (Moscow) Suppl. Ser. A Membr. Cell Biol. 6 (2012) 26–34.
[43] I. Sienaert, H. De Smedt, J.B. Parys, L. Missiaen, S. Vanlingen, H. Sipma, R. Casteels, Characterization of a cytosolic and a luminal Ca2+ binding site in the type I inositol 1,4,5-trisphosphate receptor, J. Biol. Chem. 271 (1996) 27005–27012.
[44] J.H. Horne, T. Meyer, Luminal calcium regulates the inositol trisphosphate receptor of rat basophilic leukemia cells at a cytosolic site, Biochemistry 34 (1995) 12738–12746.
[45] I. Sienaert, L. Missiaen, H. De Smedt, J.B. Parys, H. Sipma, R. Casteels, Molecular and functional evidence for multiple Ca2 + -binding domains in the type 1 inositol 1,4,5-trisphosphate receptor, J. Biol. Chem. 272 (1997) 25899–25906.
[46] L. Missiaen, H. De Smedt, J.B. Parys, R. Casteels, Co-activation of inositol trisphosphate-induced Ca2+ release by cytosolic Ca2+ is loading-dependent, J. Biol. Chem. 269 (1994) 7238–7242.
[47] D.O. Mak, S. McBride, J.K. Foskett, Regulation by Ca2+ and inositol 1,4,5-trisphosphate (InsP3) of single recombinant type 3 InsP3 receptor channels. Ca2+ activation uniquely distinguishes types 1 and 3 insp3 receptors, J. Gen. Physiol. 117 (2001) 435–446.
[48] E.J. Kaftan, B.E. Ehrlich, J. Watras, Inositol 1,4,5-trisphosphate (InsP3) and calcium interact to increase the dynamic range of InsP3 receptor-dependent calcium signaling, J. Gen. Physiol. 110 (1997) 529–538.
[49] S.K. Joseph, H.L. Rice, J.R. Williamson, The effect of external calcium and pH on inositol trisphosphate-mediated calcium release from cerebellum microsomal fractions, Biochem. J. 258 (1989) 261–265.
[50] A. Tanimura, R.J. Turner, Inositol 1,4,5-trisphosphate-dependent oscillations of luminal [Ca2+] in permeabilized HSY cells, J. Biol. Chem. 271 (1996) 30904–30908.
[51] B. Zimmermann, Control of InsP3-induced Ca2+ oscillations in permeabilized blowfly salivary gland cells: contribution of mitochondria, J. Physiol. 525 (Pt 3) (2000) 707–719.
[52] C. Camello, R. Lomax, O.H. Petersen, A.V. Tepikin, Calcium leak from intracellular stores—the enigma of calcium signalling, Cell Calcium 32 (2002) 355–361.
[53] T.J. Shuttleworth, O. Mignen, Calcium entry and the control of calcium oscillations, Biochem. Soc. Trans. 31 (2003) 916–919.
[54] A. Tanimura, T. Morita, A. Nezu, A. Shitara, N. Hashimoto, Y. Tojyo, Use of fluorescence resonance energy transfer-based biosensors for the quantitative analysis of inositol 1,4,5-trisphosphate dynamics in calcium oscillations, J. Biol. Chem. 284 (2009) 8910–8917.

[55] T. Ogawa, T. Hayashi, S. Kyoizumi, T. Ito, J.E. Trosko, N. Yorioka, Up-regulation of gap junctional intercellular communication by hexamethylene bisacetamide in cultured human peritoneal mesothelial cells, Lab. Invest. 79 (1999) 1511–1520.
[56] J.S. Davidson, I.M. Baumgarten, Glycyrrhetinic acid derivatives: a novel class of inhibitors of gap-junctional intercellular communication. Structure–activity relationships, J. Pharmacol. Exp. Ther. 246 (1988) 1104–1107.
[57] M.A. Matlib, Z. Zhou, S. Knight, S. Ahmed, K.M. Choi, J. Krause-Bauer, R. Phillips, R. Altschuld, Y. Katsube, N. Sperelakis, D.M. Bers, Oxygen-bridged dinuclear ruthenium amine complex specifically inhibits Ca2+ uptake into mitochondria in vitro and in situ in single cardiac myocytes, J. Biol. Chem. 273 (1998) 10223–10231.
[58] K. Nagasaki, S. Fleischer, Ryanodine sensitivity of the calcium release channel of sarcoplasmic reticulum, Cell Calcium 9 (1988) 1–7.
[59] B. Schwaller, Calretinin: from a "simple" Ca(2+) buffer to a multifunctional protein implicated in many biological processes, Front. Neuroanat. 8 (2014) 3.
[60] C. Doglioni, A.P. Dei Tos, L. Laurino, P. Iuzzolino, C. Chiarelli, M.R. Celio, G. Viale, Calretinin: a novel immunocytochemical marker for mesothelioma, Am. J. Surg. Pathol. 20 (1996) 1037–1046.
[61] G.C. Faas, B. Schwaller, J.L. Vergara, I. Mody, Resolving the fast kinetics of cooperative binding: Ca2+ buffering by calretinin, PLoS Biol. 5 (2007) e311.
[62] L. Pecze, W. Blum, B. Schwaller, Mechanism of capsaicin receptor TRPV1-mediated toxicity in pain-sensing neurons focusing on the effects of Na(+)/Ca(2+) fluxes and the Ca(2+)-binding protein calretinin, Biochim. Biophys. Acta 1833 (2013) 1680–1691.
[63] E. Carafoli, Calcium pump of the plasma membrane, Physiol. Rev. 71 (1991) 129–153.
[64] D.L. Schmucker, J.S. Mooney, A.L. Jones, Stereological analysis of hepatic fine structure in the Fischer 344 rat. Influence of sublobular location and animal age, J. Cell Biol. 78 (1978) 319–337.
[65] F. Van Coppenolle, F. Vanden Abeele, C. Slomianny, M. Flourakis, J. Hesketh, E. Dewailly, N. Prevarskaya, Ribosome-translocon complex mediates calcium leakage from endoplasmic reticulum stores, J. Cell Sci. 117 (2004) 4135–4142.
[66] C. Harteneck, M. Gollasch, Pharmacological modulation of diacylglycerol-sensitive TRPC3/6/7 channels, Curr. Pharm. Biotechnol. 12 (2011) 35–41.
[67] M. Ito, F. Tanabe, A. Sato, E. Ishida, Y. Takami, S. Shigeta, Inhibition of natural killer cell-mediated cytotoxicity by ML-9, a selective inhibitor of myosin light chain kinase, Int. J. Immunopharmacol. 11 (1989) 185–190.
[68] K.E. Smith, C. Gu, K.A. Fagan, B. Hu, D.M. Cooper, Residence of adenylyl cyclase type 8 in caveolae is necessary but not sufficient for regulation by capacitative Ca(2+) entry, J. Biol. Chem. 277 (2002) 6025–6031.
[69] P. Varnai, L. Hunyady, T. Balla, STIM and Orai: the long-awaited constituents of store-operated calcium entry, Trends Pharmacol. Sci. 30 (2009) 118–128.
[70] M.H. Kim, J.B. Seo, L.A. Burnett, B. Hille, D.S. Koh, Characterization of store-operated Ca2+ channels in pancreatic duct epithelia, Cell Calcium 54 (2013) 266–275.
[71] J. Sneyd, K. Tsaneva-Atanasova, V. Reznikov, Y. Bai, M.J. Sanderson, D.I. Yule, A method for determining the dependence of calcium oscillations on inositol trisphosphate oscillations, Proc. Natl. Acad. Sci. U. S. A. 103 (2006) 1675–1680.
[72] D.D. Friel, R.W. Tsien, Phase-dependent contributions from Ca2+ entry and Ca2+ release to caffeine-induced [Ca2+]i oscillations in bullfrog sympathetic neurons, Neuron 8 (1992) 1109–1125.
[73] N.M. Woods, K.S. Cuthbertson, P.H. Cobbold, Repetitive transient rises in cytoplasmic free calcium in hormone-stimulated hepatocytes, Nature 319 (1986) 600–602.
[74] T. Yada, S. Oiki, S. Ueda, Y. Okada, Synchronous oscillation of the cytoplasmic Ca2+ concentration and membrane potential in cultured epithelial cells (Intestine 407), Biochim. Biophys. Acta 887 (1986) 105–112.
[75] Y. Tsunoda, E.L. Stuenkel, J.A. Williams, Oscillatory mode of calcium signaling in rat pancreatic acinar cells, Am. J. Physiol. 258 (1990) C147–C155.
[76] T.A. Rooney, E.J. Sass, A.P. Thomas, Characterization of cytosolic calcium oscillations induced by phenylephrine and vasopressin in single fura-2-loaded hepatocytes, J. Biol. Chem. 264 (1989) 17131–17141.
[77] M. Whitaker, Genetically encoded probes for measurement of intracellular calcium, Methods Cell Biol. 99 (2010) 153–182.
[78] C. Fewtrell, Ca2+ oscillations in non-excitable cells, Annu. Rev. Physiol. 55 (1993) 427–454.
[79] G. Dupont, L. Combettes, G.S. Bird, J.W. Putney, Calcium oscillations, Cold Spring Harb. Perspect. Biol. 3 (2011).
[80] I. Bezprozvanny, J. Watras, B.E. Ehrlich, Bell-shaped calcium-response curves of Ins(1,4,5)P3- and calcium-gated channels from endoplasmic reticulum of cerebellum, Nature 351 (1991) 751–754.
[81] J. Sneyd, M. Falcke, Models of the inositol trisphosphate receptor, Prog. Biophys. Mol. Biol. 89 (2005) 207–245.
[82] T. Michikawa, J. Hirota, S. Kawano, M. Hiraoka, M. Yamada, T. Furuichi, K. Mikoshiba, Calmodulin mediates calcium-dependent inactivation of the cerebellar type 1 inositol 1,4,5-trisphosphate receptor, Neuron 23 (1999) 799–808.
[83] E. Nosyreva, T. Miyakawa, Z. Wang, L. Glouchankova, A. Mizushima, M. Iino, I. Bezprozvanny, The high-affinity calcium[bond]calmodulin-binding site does not play a role in the modulation of type 1 inositol 1,4,5-trisphosphate receptor function by calcium and calmodulin, Biochem. J. 365 (2002) 659–667.
[84] L. Missiaen, C.W. Taylor, M.J. Berridge, Luminal Ca2+ promoting spontaneous Ca2+ release from inositol trisphosphate-sensitive stores in rat hepatocytes, J. Physiol. 455 (1992) 623–640.
[85] L. Missiaen, H. De Smedt, G. Droogmans, R. Casteels, Luminal Ca2+ controls the activation of the inositol 1,4,5-trisphosphate receptor by cytosolic Ca2+, J. Biol. Chem. 267 (1992) 22961–22966.
[86] E.C. Thrower, H. Mobasheri, S. Dargan, P. Marius, E.J. Lea, A.P. Dawson, Interaction of luminal calcium and cytosolic ATP in the control of type 1 inositol (1,4,5)-trisphosphate receptor channels, J. Biol. Chem. 275 (2000) 36049–36055.
[87] G. Dupont, A. Goldbeter, One-pool model for Ca2+ oscillations involving Ca2+ and inositol 1,4,5-trisphosphate as co-agonists for Ca2+ release, Cell Calcium 14 (1993) 311–322.
[88] A.M. Hofer, B. Landolfi, L. Debellis, T. Pozzan, S. Curci, Free [Ca2+] dynamics measured in agonist-sensitive stores of single living intact cells: a new look at the refilling process, EMBO J. 17 (1998) 1986–1995.
[89] K. Ishii, K. Hirose, M. Iino, Ca2+ shuttling between endoplasmic reticulum and mitochondria underlying Ca2+ oscillations, EMBO Rep. 7 (2006) 390–396.
[90] M. Endo, Calcium release from the sarcoplasmic reticulum, Physiol. Rev. 57 (1977) 71–108.
[91] A.V. Shmigol, D.A. Eisner, S. Wray, Simultaneous measurements of changes in sarcoplasmic reticulum and cytosolic, J. Physiol. 531 (2001) 707–713.
[92] A. Dagnino-Acosta, A. Guerrero-Hernandez, Variable luminal sarcoplasmic reticulum Ca(2+) buffer capacity in smooth muscle cells, Cell Calcium 46 (2009) 188–196.
[93] M.J. Berridge, Inositol trisphosphate and calcium oscillations, Biochem. Soc. Symp. (2007) 1–7.
[94] L.E. Fridlyand, N. Tamarina, L.H. Philipson, Bursting and calcium oscillations in pancreatic beta-cells: specific pacemakers for specific mechanisms, Am. J. Physiol. Endocrinol. Metab. 299 (2010) E517–E532.
[95] F.W. Tse, A. Tse, B. Hille, Cyclic Ca2+ changes in intracellular stores of gonadotropes during gonadotropin-releasing hormone-stimulated Ca2+ oscillations, Proc. Natl. Acad. Sci. U. S. A. 91 (1994) 9750–9754.
[96] T.P. Remus, A.V. Zima, J. Bossuyt, D.J. Bare, J.L. Martin, L.A. Blatter, D.M. Bers, G.A. Mignery, Biosensors to measure inositol 1,4,5-trisphosphate concentration in living cells with spatiotemporal resolution, J. Biol. Chem. 281 (2006) 608–616.
[97] T. Matsu-ura, T. Michikawa, T. Inoue, A. Miyawaki, M. Yoshida, K. Mikoshiba, Cytosolic inositol 1,4,5-trisphosphate dynamics during intracellular calcium oscillations in living cells, J. Cell Biol. 173 (2006) 755–765.
[98] G.S. Bird, J.W. Putney Jr., Capacitative calcium entry supports calcium oscillations in human embryonic kidney cells, J. Physiol. 562 (2005) 697–706.